Thesis for the degree of Doctor of Philosophy

Design, modelling and operation of a 100 kW chemical-looping combustor for solid fuels

Pontus Markström

CHALMERS

Energy and Environment
CHALMERS UNIVERSITY OF TECHNOLOGY
Göteborg, Sweden 2012

Design, modelling and operation of a 100 kW chemical-looping combustor for solid fuels
Pontus Markström
ISBN 978-91-7385-771-0

Doktorsavhandlingar vid Chalmers tekniska högskola
Ny serie nr 3452
ISSN 0346-718X

Department of Energy and Environment
Chalmers University of Technology
SE-412 96 Göteborg, Sweden
Telephone +46-(0)31-772 1000

Chalmers Reproservice
Göteborg, Sweden 2012

Design, modelling and operation of a 100 kW chemical-looping combustor for solid fuels

Pontus Markström
Department of Energy and Environment
Chalmers University of Technology
SE-412 96 Göteborg, Sweden

Abstract

With the increasing threat of global warming, technologies for efficient capture and storage of the greenhouse gas CO_2 are sought after. Chemical-looping combustion is a novel CO_2 capture technology that can be applied when burning gaseous, liquid or solid fuels. By using two interconnected fluidised beds with a bed material capable of transferring oxygen from air to the fuel, a nitrogen-undiluted stream of CO_2 can be obtained with no direct efficiency loss. This thesis is focused on design, modelling and operation of a 100 kW chemical-looping combustor for solid fuels. The goal of the test rig is validation of chemical-looping combustion at a scale giving both high operational flexibility and semi industrial conditions.

Two analytical models that can be applied to any chemical-looping combustor for solid fuels are presented. The first model finds the residence-time from batch-experiments. The second model estimates the gas conversion of a general fuel as a function of the oxygen carrier bed inventory. Furthermore, a cold-flow model of the 100 kW unit has been constructed. Details about the cold-flow model design and experimental results regarding fluidisation, slugging, residence-time and circulation are presented.

The 100 kW unit has been operated for over 23 hours with an ilmenite oxygen carrier, using three different fuels. During this time, no instabilities in the bed inventories have been detected. Experiments aiming for optimal performance showed that gas conversion above 84% and CO_2 capture over 99% are possible. A detailed analysis of the relation between the global solids circulation, the fuel reactor bed inventory and the gas conversion was conducted. The results revealed that the bed inventory in the fuel reactor had a strong impact on gas conversion, whereas little effect of overall circulation could be seen under the present conditions.

Keywords: Carbon capture and storage; Chemical-looping combustion; CO2 capture; Fluidised beds; Oxygen carriers; Modelling

Publications

This thesis consists of an introductory text and the following six appended research papers, henceforth referred to as Paper I–VI:

I. P. Markström, N. Berguerand and A. Lyngfelt. The application of a multistage-bed model for residence-time analysis in chemical-looping combustion of solid fuel. *Chemical Engineering Science*, 65(18):5055–5066, 2010.

II. P. Markström and A. Lyngfelt. Designing and operating a cold-flow model of a 100 kW chemical-looping combustor. *Powder Technology*, 222:182–192, 2012.

III. P. Markström, A. Lyngfelt and C. Linderholm. Chemical-looping combustion in a 100 kW unit for solid fuels. In *21st International Conference on Fluidized Bed Combustion*, volume 1, pages 285–292, Naples, Italy, 3–6 June 2012.

IV. P. Markström, C. Linderholm and A. Lyngfelt. Operation of a 100 kW chemical-looping combustor with Mexican petroleum coke and Cerrejón coal. In *2nd International Conference on Chemical Looping*, Darmstadt, Germany, 26–28 September 2012.

V. P. Markström, C. Linderholm and A. Lyngfelt. Chemical-looping combustion of solid fuels – Design and operation of a 100 kW unit with bituminous coal. *Submitted for publication in International Journal of Greenhouse Gas Control*, 2012.

VI. P. Markström, C. Linderholm and A. Lyngfelt. Modelling gas conversion in a 100 kW chemical-looping combustor for solid fuels. *Submitted for publication in Chemical Engineering Science*, 2012.

Contribution

I. First author, responsible for data evaluation and writing.

II. First author, responsible for experimental work, data evaluation and writing.

III. First author, shared responsibility for the experimental work, responsible for data evaluation and writing.

IV. First author, shared responsibility for the experimental work, responsible for data evaluation and writing.

V. First author, shared responsibility for the experimental work, responsible for data evaluation and writing.

VI. First author, shared responsibility for the experimental work, responsible for data evaluation and writing.

Related publications not included in the thesis

- N. Berguerand, A. Lyngfelt, T. Mattisson and P. Markström. Chemical-looping combustion of solid fuels in a 10 kW_{th} unit. *Oil & Gas Science and Technology – Rev. IFP Energies nouvelles*, 66(2):181–191, 2011.
- M. Rydén, C. Linderholm, P. Markström and A. Lyngfelt. Release of gas phase O_2 from ilmenite during chemical-looping combustion experiments. *Chemical Engineering & Technology*, 35(11):1968–1972, 2012.

Acknowledgements

First and foremost, I would like to thank my supervisor, Prof. Anders Lyngfelt. Being completely new to this area of science, I am grateful for the perfect mix of patience, guidance and responsibility you have given me. I am also grateful to my co-supervisor, Prof. Tobias Mattisson, for all the support.

Also, a big thank you to all the employees at the division of Energy Conversion for providing a great working atmosphere, especially the past (and present) chemical-loopers: Nicolas Berguerand, Carl Linderholm, Patrick Moldenhauer, Magnus Rydén, DaZheng Jing, Golnar Azimi, Mehdi Arjmand, Henrik Leion, Peter Hallberg, Erik Jerndal, Martin Keller, Sebastian Sundqvist, Jesper Aronsson, Matthias Schmitz, Malin Källén and Ulf Stenman.

A special mention goes to the following people. Nicolas: the collaboration in Paper I was great. Thanks for being such a good friend in spite of my bad Swedish/French jokes ;). Calle: it is a pleasure to listen to your clear way of thinking. Thank you for the collaboration in Papers III–VI. Ulf: my experiences working with you in the lab have been invaluable. It is always a pleasure talking to you, not to mention listening to your mantra!

I would also like to thank my financers, the Research Fund for Coal and Steel of the European Community, Alstom Power Boilers, Carl Trygger's Foundation for Scientific Research, J. Gust. Richert Memorial Fund and Ångpanneföreningen's Foundation for Research and Development.

Finally, I want to thank my family for all the support over the years: my parents, my brother Jan and my sister Pia for being such a loving and special family, Lei and Baoyi for all the wonderful dinners and Ling for all the love and encouragement.

Contents

Outline

This thesis is based on six papers in the field of chemical-looping combustion. A brief overview of the chapters in this thesis are given below.

In **Chapter 1**, the introduction presents arguments as to why research in this field is important. Here, the problem of global warming due to greenhouse gas emissions is discussed, as well as a background to carbon capture and storage. It also provides a summary of the field of research and an introduction to chemical-looping combustion, including the basic chemical reactions that take place in the reactor system.

Chapter 2 describes the design of two chemical-looping combustors, a 10 kW (Paper I) and a 100 kW (Paper III–VI), for solid fuels as well as basic definitions used in the data evaluation. Here, important properties of the oxygen carrier and the fuels are summarised. The focus in the discussion lies on the 100 kW unit. Furthermore, a theoretical background of a cold-flow model (Paper II), built to simulate the 100 kW unit, with an overview on design and calculations of the dynamic similarity, is provided.

Chapter 3 involves different aspects of modelling of chemical-looping combustion for solid fuels. Just as in the previous chapter, it focuses on two sizes of reactor systems. The 10 kW and the 100 kW unit. The modelling in the 10 kW unit describes a general procedure to estimate the residence time and global solids circulation in a chemical-looping combustor fed with solid fuels. From analyses of gas leaving the air reactor, it was possible to determine the residence-time and residence-time distribution of particles in the fuel reactor. From the known solids inventory in the fuel reactor, the circulation mass flow could be directly correlated to measured operational data, i.e. pressure drop, temperature and gas flow in the air reactor riser. The modelling also contains the experimental evaluation of the cold-flow model system. Studies were made on the mass flows, mass fluxes and residence-times in the air and fuel reactors using air as fluidisation gas. Finally, an analytical model for gas conversion of solid fuels is presented. The model is based on the bed inventory of the fuel reactor in the 100 kW unit and is applied to the case of a bituminous coal and ilmenite oxygen carrier.

In **Chapter 4**, results from operation in the 100 kW unit are presented. It describes experiments conducted with three fuels, focusing on the design fuel, a bituminous coal from Colombia: Cerrejón coal. In total, over 23 hours of operation have been analysed.

Finally, in **Chapter 5** the results from all the papers are summarised and the conclusions are discussed.

1

Introduction

1.1 Global warming

In recent years, the greenhouse effect has gained a lot of attention due to alarming reports of global warming. Instrumental recordings over the past 157 years show that temperatures at the surface have risen globally in two main phases [1]. In the first phase, from the 1910s to the 1940s, the average temperature rose 0.35℃ and in the second phase, from the 1970s to the 2000s, the average temperature rose 0.55℃, see Fig. 1.1. In addition, 11 of the 12 warmest years on record have occurred in the past 12 years.

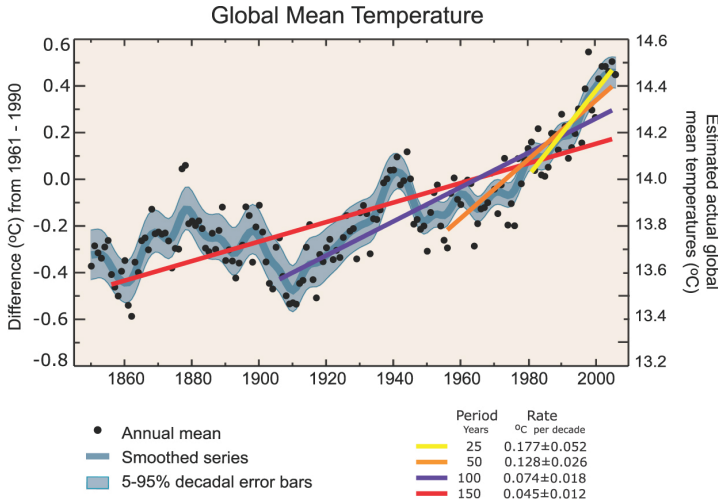

Fig. 1.1: Annual global mean observed temperatures, from [1].

In addition to the increase in global average surface temperature, many indications of global warming exist. The increase in global average sea level and the decrease in the northern hemisphere snow cover are such indications. If the global mean temperature continues to increase, it will lead to serious changes in the climate that may cause irreversible harm to ecological systems. A major part of the scientific community today agrees that the cause of global warming is an anthropogenic greenhouse effect, rather than a natural process. As combustion of fossil fuels results in large emissions, it was natural to envisage

a correlation between increased temperatures and an increased production of greenhouse gases.

The greenhouse effect has been named from the process occurring in a greenhouse with glass walls, where the temperature of the air inside is increased. The effect occurring on Earth is analogous in the sense that both the glass and the greenhouse gases in the atmosphere may transmit short-wave radiation from the sun, but absorb long-wave (infrared) radiation from the ground. The process on Earth can be described in the following way: From the sun, radiation in all wavelengths is emitted continuously. Approximately 1/3 of the radiation that reaches the Earth is reflected in the atmosphere back to space, 1/6 is absorbed in the atmosphere and about 1/2 is absorbed by the Earth's surface, making it warmer [2]. The warmed surface radiates heat through infrared radiation. Greenhouse gases in the atmosphere, predominantly water vapor (H_2O) and carbon dioxide (CO_2), absorbs and re-emits most of this radiation in all directions, including back to Earth. This effect creates a situation where trapped infrared radiation, or heat, warms the Earth's surface and the lower atmosphere. Other gases present in the atmosphere, e.g. methane (CH_4), nitrous oxide (N_2O) and ozone (O_3), also contribute to the greenhouse effect. The three most important greenhouse gases that not only originate from natural processes, but also from industrial emissions, are CO_2, CH_4 and N_2O. More than 60 other greenhouse gases, in groupings of hydrofluorocarbons, perfluorinated compounds, fluorinated ethers and other hydrocarbons are present in the atmosphere, but only in minute concentrations [3]. Both CH_4 and N_2O are much more effective as greenhouse gases compared to CO_2. However, as the concentration of CO_2 in the atmosphere is in the order of 1000 times higher than the other two (ppm instead of ppb) and because it is completely dominant in the flue gases from fossil fuel combustion, it has become the centre of attention when discussing greenhouse gas emissions. The historical concentration of these three greenhouse gases in the atmosphere can be measured indirectly by analysing trapped gas pockets in the polar ice caps, dating back thousands of years. Combining averages from such analyses with modern measurements reveals a drastic change, caused by emissions from anthropogenic processes, see Fig. 1.2. Industrial development across the world continues

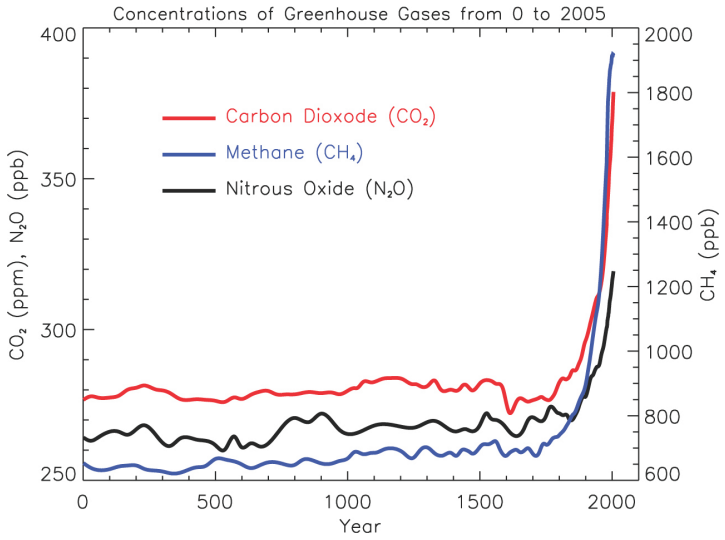

Fig. 1.2: Atmospheric concentrations of important long-lived greenhouse gases over the last 2000 years, from [3].

to increase the greenhouse gas emissions, which in turn may lead to increased temperatures at the surface of the Earth. This in turn leads to increased evaporation of water from the oceans, and thus increased concentration of water vapor in the atmosphere. As water vapor is a powerful greenhouse gas, the greenhouse effect becomes self-reinforced. It is believed that this water vapor feedback may in fact double the increase in the greenhouse effect due to the added CO_2 [2].

According to the Copenhagen Accord [4], the increase in global temperature should be kept below 2°C in order to prevent dangerous anthropogenic interference with the climate system. To meet this target, countries need to drastically cut their emissions of greenhouse gases. Due to the rapidly increasing demands of energy around the world, it is, in practice, difficult to phase out the usage of fossil fuels quickly enough by replacing it with non-fossil energy sources like wind, solar or nuclear power. Consequently, the CO_2 resulting from combustion processes would need to be removed. A possible solution is to use carbon capture and storage (CCS). This concept can be used as a bridge to a more long-term solution, in which renewable energy sources can take over. However, due to the energy demand in the capture process, CCS involves a cost. This thesis studies a capture technology called chemical-looping combustion (CLC). Chemical-looping combustion is a novel combustion process for gaseous, liquid or solid fuels, producing a pure stream of CO_2 without any direct efficiency loss.

1.2 Carbon capture and storage

Technologies that enable the possibility for combustion without nitrogen-diluted exhaust gas have in recent years received more and more attention, and several methods to capture and store the CO_2 are investigated. The concept has been applied in various locations around the world and is now considered to be an important option for decelerating the increase of atmospheric CO_2. Most information in Section 1.2 is adapted from [5] unless otherwise stated.

1.2.1 Capturing the CO_2

The larger stationary sources that are mostly responsible for anthropogenic CO_2 emissions are power plants, cement production and steel production plants. For example, in 1995, more than 1400 Mt CO_2 were released in steel production associated emissions. Other processes like natural gas sweetening, which is a separation method for CO_2 contaminated natural gas, also produce large amounts of CO_2. There are ways to capture the CO_2, many of which are directed towards combustion systems. Below, a brief summary of the main CO_2 capture technologies is provided. In these examples, the CO_2 is generated in large-scale combustion processes using fossil fuels.

- Post-combustion: Here, the CO_2 rich flue gas is treated downstream of the combustion process. Examples of post-combustion capture processes are absorption processes, adsorption processes, membranes and solid sorbents. The most common ones are the absorption processes, which use the reversibility of chemical reactions to capture and then release the CO_2. By letting a solvent be brought in contact with the flue gas, CO_2 will be absorbed. The solvent is then regenerated and CO_2 is released in a stripper at 100–140°C. This leads to a drop in efficiency as this temperature

needs to be maintained. Using the absorption process, typically 80–95% of the CO_2 is recovered. Usually an amine is used, but recently, chilled ammonia has received a lot of attention. The chilled ammonia process uses an aqueous ammonium solution at 0–10℃ to capture CO_2 by forming ammonium bicarbonate [6].

- Oxy-fuel combustion: By separating the oxygen from air and using it directly in a combustion process, it is possible to produce flue gases free from nitrogen dilution. After subsequent steps of steam condensation and cleaning of impurities, such as argon, NO_x and SO_x, a pure stream of CO_2 can be obtained. Methods of air separation techniques include e.g. cryogenic distillation, adsorption using multi-bed pressure swing units, and polymeric membranes. To keep the temperature down in the combustion chamber, the oxygen is diluted on purpose with recycled CO_2 rich flue gas. This process has an efficiency drop due to the air separation process, but may potentially capture close to 100% of all CO_2.

- Pre-combustion: This process is essentially a method of producing hydrogen from a hydrocarbon or carbonaceous fuel with the help of steam. As the bi-product in this production is CO_2, pre-combustion is a very convenient alternative for CO_2 capture. By letting the hydrocarbon react with either steam or oxygen in sub-stoichiometric amounts, syngas (H_2 and CO) is produced. The first method is called steam reforming and the latter is called partial oxidation or gasification, depending on if the fuel is gaseous/liquid or solid, respectively. Finally, by adding more steam, the water-gas shift reaction,

$$CO + H_2O \leftrightarrow CO_2 + H_2, \tag{1.1}$$

  can be used to push the CO to CO_2. This CO_2 can then be captured in a subsequent separation step. The separation step may use e.g. pressure swing adsorption or an absorbing amine solvent. Hence, this capture technology shares the efficiency drop with the post-combustion and oxy-fuel combustion processes. Pre-combustion may also involve a chemical-looping technology (see below), in a process called chemical-looping reforming [7, 8].

- Unmixed combustion: An alternative to the technologies presented above, all involving costly and energy consuming gas separation. In these technologies, fuel and air are never mixed. There are two such technologies, chemical-looping combustion and fuel cells.

1.2.2 Storing the CO_2

It is not clear today as to how long the CO_2 need to remain in storage. It depends on factors such as the maximum atmospheric concentration of CO_2 that is set as a policy goal, the timing of that maximum, the anticipated duration of the fossil fuel era, and available means of controlling the CO_2 concentration in the event of significant future releases. Just as for the capture process, there are several alternatives to store the CO_2 captured from the technologies previously mentioned. Three examples of storage technologies are on and off-shore geological storage, ocean storage and mineral carbonation.

The one that shows most promise is geological storage. This is due to research showing that is very likely that over 99% will be retained over 100 years and likely that over

99% will be retained over 1000 years. In geological storage, the CO_2, compressed to its supercritical state, is injected into geological formations under ground. Geological storage locations could be e.g. oil fields for enhanced oil recovery, gas fields, or porous rocks such as sandstone reservoirs.

The most prominent example for enhanced oil recovery is the Weyburn CO_2–EOR project, which started in late 2000. Here, CO_2 at a rate between 1.1–1.8 Mt/yr is injected into a 180 km^2 fractured carbonate oil reservoir, expected to store 20 Mt in total.

Sandstone reservoirs are in use in several commercial scale projects across the world today. Their use as geological storage for CO_2 is often connected to a gas field, where natural gas is taken from large production wells. As the gas will contain an amount of unwanted CO_2, it will undergo a separation process that captures the CO_2. This CO_2 is then injected into a sandstone reservoir, either beneath, above, or into the original gas field. Two successful projects with sandstone reservoirs are given below.

- The first storage site began its operation in 1996. This was when Statoil started the off-shore Sleipner CO_2 storage project in the North-Sea, 250 km off the coast of Norway. The Sleipner project is located in the south of the Utsira formation, a saline aquifer with a surface area of 26000 km^2, 800–1000 m below the sea floor. CO_2 is injected into the sandstone reservoir, located above a natural gas field, from an ocean platform at a rate of approximately 1 Mt/yr.

- Another example is BP's In Salah gas project in the central Saharan region of Algeria. Here, the CO_2 is injected into the same sandstone reservoir as the natural gas is produced from. However, the production wells and the injection wells are separated in such a way that a migration of CO_2 to the gas field will happen long after depletion of the gas zone. 17 Mt of CO_2 will be stored here at a rate of up to 1.2 Mt/yr. Operation started in 2004 and the CO_2 is injected at a depth of 1800 m.

In ocean storage, there are several proposals available. One proposal is to inject the CO_2 below 3 km depth, where CO_2 is denser than sea water. This leads to the formation of CO_2 lakes at the bottom of the seafloor. A second proposal is to inject the CO_2 somewhere between 1–3 km depth. Then the CO_2 will form an upward plume, dissolving into the seawater on its way up. Here, research shows that 65-100% will be retained after 100 years and that 30-85% will be retained after 500 years, depending on if the depth of injection was closer to 1000 m or 3000 m. Because of the poor retention, the interest in ocean storage is moderate.

Mineral carbonation involves converting CO_2 to solid inorganic carbonates, which are geologically stable. This may be accomplished from chemical reactions between CO_2 and silicate minerals containing magnesium and calcium. Mineral carbonation is at an early stage of development and the feasibility of such a process is uncertain, but it has the advantage of highly irreversible CO_2 retainment.

1.3 Chemical-looping combustion

1.3.1 Concept

As discussed in Section 1.2, regular combustion uses air to burn the fuel, where the CO_2 produced is diluted with nitrogen. Technologies that use different forms of gas separa-

tion are being studied, but will inevitably lead to a drop in efficiency. In this aspect, chemical-looping combustion is relevant. As a carbon-capture technology with inherent capture of CO_2, chemical-looping combustion is both feasible and fully compatible with the new storage technologies. The defining feature of chemical-looping combustion is the circulation of oxygen carrier particles between two main reactors. In one of these main reactors, air is introduced from below. Here, the particles become oxidised in exothermal reactions as they are fluidised. Hence, this reactor is normally called the air reactor. The particles are then transported through a loop seal, entering the other main reactor. As this reactor is where the fuel is inserted, it is called the fuel reactor. Depending on the kind of fuel used, this reactor could be fluidised with either steam, CO_2 or the fuel itself. The fuel then reacts with oxygen available in the particles, which become reduced. Loop seals prevent gases between the air and fuel reactor to mix, and hence the net effect of the process is a transport of oxygen to the fuel reactor with no nitrogen dilution and without any direct efficiency loss. After subsequent steps of steam condensation and gas cleaning from e.g. sulphur compounds, a pure stream of CO_2 is obtained. This CO_2 can then be transported to a suitable location for storage.

1.3.2 Operation with gaseous fuels

The concept of chemical-looping combustion, as described in Section 1.3.1, is depicted in Fig. 1.3. It shows the oxygen carrier as a metal oxide, labelled Me_xO_y in oxidised form and Me_xO_{y-1} in reduced form. Burning e.g. natural gas or syngas, the fuel itself is used as the fluidisation medium in the fuel reactor. For gaseous fuels in the form of various

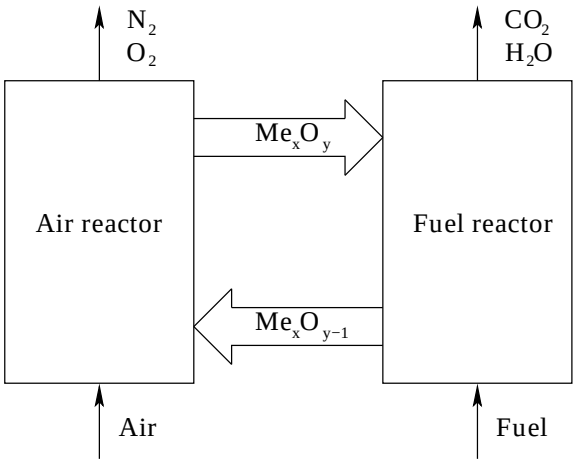

Fig. 1.3: Principal sketch of the CLC process with an air and a fuel reactor, interconnected to allow an exchange of oxygen-carrier material.

hydrocarbons, the resulting chemical reactions (1.2) and (1.3) describe the processes in the fuel and air reactor, respectively.

$$C_nH_{2m} + (2n+m)Me_xO_y \rightarrow nCO_2 + mH_2O + (2n+m)Me_xO_{y-1} \quad (1.2)$$

$$O_2 + 2Me_xO_{y-1} \rightarrow 2Me_xO_y \quad (1.3)$$

A fuel like natural gas often consists of more than 90% methane. In addition, it also contains ethane, propane, butane, carbon dioxide, nitrogen, and sometimes sulphuric com-

pounds that may lead to SO_2 emissions. However, as the combustion does not involve high temperature flames, there will be no thermal NO_x production. The reactions above show that the only products of sulphur-free hydrocarbon combustion should be steam and CO_2.

1.3.3 Operation with with solid fuels

The method of feeding solid fuels into a chemical-looping combustor is a bit different compared to using gaseous fuels. Clearly, the fuel cannot be fed in the same fashion as indicated in Fig. 1.3. Instead, two other options are available [9]. The fuel can either be fed from above in the fuel reactor, or it can fed into the bed directly. Releasing the fuel above the bed has a major drawback in that the release of volatiles may occur before they have had the time to react with the oxygen carriers. If these volatiles leave the system with the flue gases, un-reacted, they need to be burnt in an oxy-fuel process further downstream, which in turn leads to increased costs. Therefore, in-bed feeding is preferred. For solid fuels with in-bed feeding, the volatiles content will react according to (1.2), but the char needs to be gasified since no direct solid-solid reaction between the fuel and oxygen carrier can be expected. In this step, the char must first react with steam (1.4) or carbon dioxide (1.5) to form combustible gas,

$$\mathrm{C} + \mathrm{H_2O} \rightarrow \mathrm{CO} + \mathrm{H_2} \tag{1.4}$$

$$\mathrm{C} + \mathrm{CO_2} \rightarrow 2\mathrm{CO}. \tag{1.5}$$

The resulting H_2 and CO then react according to

$$\mathrm{H_2/CO} + \mathrm{Me}_x\mathrm{O}_y \rightarrow \mathrm{H_2O/CO_2} + \mathrm{Me}_x\mathrm{O}_{y-1}, \tag{1.6}$$

i.e. yielding steam and CO_2 as end products. However, there will also be sulphuric emissions, mostly in the form of SO_2 and H_2S. The levels depend on the kind of solid fuel used, i.e. on the amounts of elemental sulphur present in the fuel. For some fuels like South African coal, it can be relatively moderate levels (< 1 wt%), while for others like Mexican petroleum coke, the sulphur content can be over 6 wt% [10]. Another difference compared to gaseous fuels is that solid fuels always contain a certain amount of ash. These differences, together with the fuel feeding, makes chemical-looping combustion with solid fuels more complicated than with gaseous fuels. As for gaseous fuels, there will be no thermal NO_x production with solid fuels. However, fuel nitrogen will contaminate the gas from the fuel reactor as e.g. N_2 and NO.

1.3.4 Operation with liquid fuels

The challenge of feeding liquid fuels is similar to feeding solid fuels. Any fuel needs to be in gas phase before reactions with the oxygen carrier can take place. Hence, the liquid fuel needs to be evaporated before it is injected into the fuel reactor. Liquid fuels can be anything from thin distillation products of petroleum, like kerosene, to heavy oils, like crude oil. As operation with liquid fuels in chemical-looping combustion is still in its infancy, experience from the feeding process is limited. One way this has been accomplished is by mixing the liquid fuel with superheated steam at the moment of injection [11]. The steam will evaporate the liquid, resulting in a mixture of steam and gaseous fuel that enters the

bed together. The hydrocarbon content of the evaporated fuel will then convert to steam and CO_2 according to reaction (1.2).

1.3.5 Development

The chemical-looping combustion principle was patented by Lewis and Gilliland [12] for use in the production of high purity CO_2 from fossil fuels. However, the process was not commercialised and was not called chemical-looping combustion. The name "chemical-looping" was given by Ishida et al. [13] as a reference to the analogous human cardiovascular system, confining chemical reactions in circulation. Soon after, Ishida and Jin [14] recognised the concept as a possibility to capture CO_2 from fossil fuels in order to reduce climate impact. The first tentative chemical-looping combustion design based on the circulating fluidised bed principle was presented by Lyngfelt et al. [15]. More than 900 materials have been investigated as possible oxygen carrier materials for this process, mostly including active oxides of iron, nickel, copper and manganese [16].

Up until the first half of 2011, reported operation for more than 4000 h had been accomplished in 12 units of 0.3–140 kW [17]. This time of operation consists mostly of operation with gaseous fuels, as they were the first to be tested. During the last few years, more focus has been put on solid and, most recently, liquid fuels. However, liquid fuels have only been tested in relatively small lab units [11, 18]. So far, reports on roughly 120 h of operation with three different oxygen carriers have been presented [11, 19]. For solid fuels, both lab investigations [20–27] as well as studies in continuous operation have been made. Examples with continuous operation are:

- A 1 kW unit for coal and biomass [28, 29]
- A 0.5–1.5 kW unit for coal [30, 31]
- A 10 kW unit for coal and petroleum coke [9, 32, 33]
- A 10 kW unit for coal and biomass [34, 35]
- A 10 kW unit for coal, methane and syngas [36]
- A 25 kW unit for lignite dust [37]
- A 25 kW unit in "coal direct chemical-looping" (CDCL) with moving beds [38, 39].

Except for the CDCL unit, these units all use their fuel reactor as a bubbling fluidised bed. This thesis concern a 100 kW unit, having tested two bituminous coals and one petroleum coke. The main difference between this unit and the previously mentioned smaller units is the possibility to use the fuel reactor as a circulating fluidised bed. Recent reviews summarise the progress in chemical-looping technologies [40–42].

Since the first design based on the circulating fluidised bed principle in 2001, chemical-looping combustion has gone from lab scale to include not only pilot scale, but also larger prototypes. The largest chemical-looping combustors today are the 1 MW_{th} unit at the Technical University of Darmstadt, Germany [43] and Alstom's 3 MW_{th} unit in Windsor, USA [44]. However, still larger units are planned [45, 46]. It is believed that chemical-looping with limestone-based oxygen carriers will scale up to demonstration size plants (10–50 MW_{el}) between the years 2015–2020, and to commercial scale ($>$ 100 MW_{el}) between the years 2020–2025 [44]. In 2005, a techno-economic study was made concerning the feasibility of a 455 MW_{el} solid fuel fired chemical-looping plant [47]. Here, it was shown that the proposed CO_2 capture power plant had a net efficiency of 41.6%, 2.3%

lower than the reference power plant, using a bituminous coal as fuel. Based on estimated investment and operation costs, the CO_2 avoidance cost for such a plant was calculated to around 10 €/tonne captured CO_2.

1.3.6 Cold-flow modelling of fluidised beds

Detailed fluid-dynamical investigations of large-scale fluidised beds can be carried out in small-scale cold-flow models at ambient conditions. This means that it is important to know if experimental results from them can accurately predict the conditions of the corresponding large-scale reactors. A cold-flow model can be made in a transparent acrylic glass, enabling a clear view of the fluidisation and mixing behaviour.

When designing experimental models to simulate the dynamics of larger units, dimensional analysis is a powerful tool. Dimensional analysis provides the scaling laws between a model and a target prototype such that the two systems will exhibit dynamically similar behaviour. Two methods to approach dimensional analysis are

- Buckingham's π-theorem [48].
- The method of non-dimensionalising the governing equations and boundary conditions.

If both of these methods are treated correctly, they will lead to the same result, i.e. the same set of dimensionless parameters. In 1984 an important paper was released by Glicksman [49], where the second method was applied to the equations of motion for a continuum model of fluids and solids phases [50]. Here, a full set of scaling relations was systematically developed, allowing a bed operating at ambient conditions to model a bed at elevated temperature and pressure. However, as this set of scaling laws constrained the dimensions of the model relative to the full scale bed, simplified versions were also developed. Glicksman identified two regions, where the scale constraint of the full set could be relaxed. They where:

- The viscous dominated region, for beds with small particles and and low velocities, where the gas inertial effects are negligible.
- The inertial dominated region, for beds with large particles at high velocities, where the gas viscous effects should be minimal

This identification led to two sets of simplified scaling laws, each valid in its respective region. Two years later, in 1986, Horio et al. [51] developed bubbling bed scaling laws that differed from the ones developed by Glicksman. However, in 1988 it was shown that the scaling laws by Horio were the same as Glicksman's simplified scaling laws in the viscous limit [52]. In 1989, Horio enhanced his previous set of scaling laws to describe a circulating fluidised bed [53]. The approach was based on the so-called "clustering annular flow model", where particle clusters move upward in the core and downward in the annulus at the wall. In 1993, Glicksman published a paper where he proposed a new set of simplified scaling laws, valid in both the viscous and the inertial dominated region at the same time [54]. The purpose was to reduce the number of scaling parameters from the two older simplified sets in the 1984 paper and to find one simplified set of scaling parameters which would be valid over a wide range of Reynolds numbers. A review paper by Glicksman in 1994 [55] summarises the research of dynamic similarity in fluidisation

and presents detailed comparisons between experiments conducted in full scale beds and experiments conducted in models, based on both the original full set of scaling laws as well as the new set of simplified scaling laws. Here, it is claimed that Horio's scaling laws from 1989, for circulating fluidised beds, can be shown to be equivalent to Glicksman's new simplified set of parameters.

Glicksman's scaling laws are today recognised as the standard approach for scaling fluidised beds and countless experiments have verified their validity. However, cases exist where they are not always successful. A good example is an early test of the full set of scaling laws performed by Fitzgerald et al. [56]. Here, differences, larger than anticipated, were measured between experimentally determined factors and theoretical values. However, the comparison still showed qualitative agreement and the differences were thought to be due to electrostatic effects and a lack of pressure measurements in order to accurately represent local dynamics.

Cold-flow models of fluidised beds can be used for many purposes. One example is to investigate the effect of the exit geometry on the flow pattern in a circulating fluidised bed riser [57]. In [57], a 1:9 scale cold-flow model, scaled using Glicksman's simplified set of scaling laws, modelled a 12 MW circulating fluidised bed-boiler. In a review article on the scale-up of fluidised-bed combustion by Leckner et al. [58], the impact of the cyclone is discussed. As the cyclone efficiency plays a significant role for the burnout of char and as an increase in cyclone efficiency extends the residence time of the char, cyclones need to be scaled correctly in order to keep the efficiency. Here, it is suggested that in geometrically similar cyclones with similar gas and particles, Stokes number scaling could be applied. Hence, for these kinds of cyclones, Stokes number should be kept the same for dynamic similarity. With respect to chemical-looping combustion, a cold-flow model of a 120 kW pilot rig for gaseous fuels was built and operated in order to study the fluid dynamics [59]. Furthermore, Paper II in this thesis studies the fluid dynamics of a 100 kW pilot rig for solid fuels.

1.3.7 Oxygen carriers

A substantial part of the research in chemical-looping combustion is focused on testing new oxygen carriers. This is understandable, considering the major role it plays in the chemical-looping process. There are many important factors to consider when choosing an oxygen carrier, such as oxygen-transfer capacity, reactivity with the fuel and oxygen, cost, health and environmental impacts, thermodynamic properties and melting point. The oxygen carriers are often manufactured, using either freeze-granulation, spray-drying, impregnation, co-precipitation or spin-flash drying. Manufactured oxygen carriers are normally metal oxides, with or without a support material to increase mechanical stability. However, they could also be natural ores or industrial by-products.

Using thermodynamic analysis, Jerndal et al. [60] showed that the metal oxides Fe_2O_3/Fe_3O_4, Cu_2O/Cu, Mn_3O_4/MnO and NiO/Ni appear to be the most suitable ones for natural gas. In a paper by Mattisson et al. [61], gas conversion using materials based on Ni, Mn and Fe were tested with CO, H_2 and CH_4. It was concluded that the reactivity of Mn and Fe-based particles with syngas was much higher than with methane. As for Ni-based oxygen carriers, Leion et al. [62] showed that the reactivity of NiO particles were considerably lower for high-sulphur fuel compared to low-sulphur fuel. This indicates that Ni-based oxygen carriers are deactivated by the presence of sulphur. In this respect, Mn

and Fe-based particles are preferred when using solid fuels.

Some oxygen carriers have shown an ability to spontaneously release oxygen in a process known as CLOU (Chemical-Looping with Oxygen Uncoupling) [63]. A CLOU particle needs to react reversibly with gas-phase oxygen at high temperature, i.e. they must be able to take up oxygen in the air reactor and release it in the fuel reactor. This means that CLOU relies on oxygen carriers that release and take up oxygen at a certain partial pressure of gas-phase oxygen and temperature. An example of a CLOU material is CuO/Cu_2O. As shown in [63], this oxygen carrier has an equilibrium oxygen partial pressure of 0.02 bar at 913℃. This means that at this temperature, oxygen will be released up to an oxygen concentration of 2% in the fuel reactor. As the partial pressure of oxygen is close to zero in the presence of fuel, a rapid release of oxygen is possible. This makes CLOU especially interesting for chemical-looping combustion with solid fuels. Except for Cu-based particles [31], many more materials have shown promising results [64, 65].

Durability of oxygen carriers with natural gas has also been tested extensively, e.g. in [66], where NiO/Ni oxygen carriers were subject to operation for more than 1000 hours. For a thorough break-down of all tested oxygen carriers up to 2010, see Adánez et al. [40]. The oxygen carrier in Papers I–VI is a 94.3% pure iron-titanium oxide called ilmenite (reduced form: $FeTiO_3$). In its oxidised state, the oxygen carrier is pseudobrookite+rutile (Fe_2TiO_5+TiO_2). However, this form is henceforth called oxidised ilmenite for simplicity.

2

Design

2.1 Oxygen carrier (Papers I–VI)

For Papers I–II, it was necessary to make a detailed analysis of some of the available literature concerning the structure and density of ilmenite. When fresh ilmenite particles are used, they need several cycles before they show stable oxidation-reduction behaviour. In addition, as the particles circulate in the system, as indicated in Fig. 1.3, and oxidise/reduce in each cycle, their density will decrease. This initial process is called *activation* and may be due to a chemical migration of the elements in ilmenite [67]. As the particles are oxidised and subsequently reduced in each cycle, the internal structure may be altered and new compounds may be formed. This may explain the formation of a more porous structure and thus lower density. With no migration, reduced ilmenite reacts in the air reactor to its most oxidised form according to

$$4\mathrm{FeTiO_3} + \mathrm{O_2} \rightarrow 2\mathrm{Fe_2TiO_5} + 2\mathrm{TiO_2}. \tag{2.1}$$

However, at the surface of activated ilmenite, an external shell enriched with hematite ($\mathrm{Fe_2O_3}$) has been found that would significantly change the thermodynamic properties of ilmenite [67]. If the oxidised ilmenite reorganises to a hematite shell and rutile ($\mathrm{TiO_2}$) core structure during activation according to

$$\mathrm{Fe_2TiO_5} + \mathrm{TiO_2} \rightarrow \underset{shell}{\mathrm{Fe_2O_3}} + \underset{core}{2\mathrm{TiO_2}}, \tag{2.2}$$

then, if the rutile core is inert, the subsequent reduction may instead produce surface magnetite ($\mathrm{Fe_3O_4}$). For the remaining cycles, oxidation would then follow

$$4\mathrm{Fe_3O_4} + \mathrm{O_2} \rightarrow 6\mathrm{Fe_2O_3} \tag{2.3}$$

instead of (2.1). The heat balance in the fuel reactor will depend on whether it is reaction (2.1) or (2.3) that occurs in the air reactor. This is due to the different enthalpies of reaction, -444.82 kJ/mol $\mathrm{O_2}$ or -480.42 kJ/mol $\mathrm{O_2}$ at 950°C, respectively. What is also affected is the oxygen transfer capacity,

$$R_0 = \frac{m_{0,ox} - m_{0,red}}{m_{0,ox}}, \tag{2.4}$$

where $m_{0,ox}$ and $m_{0,red}$ are the masses of a *fully* oxidised and a *fully* reduced oxygen carrier, respectively. With reaction (2.1), $R_0 = 0.0501$ kg O_2/kg oxidised ilmenite, while with reaction (2.3), $R_0 = 0.0334$ kg O_2/kg hematite. As the molar weight of Fe_2O_3 is almost exactly the same as for $2TiO_2$, reaction (2.2) indicates that there is maximum 0.5 kg hematite/kg oxidised ilmenite. Hence, it is likely that $1.7 \leq R_0 \leq 5.0$ wt% for activated ilmenite. This uncertainty range in R_0 is considered in Paper I and is supported by Adánez et al. [68], who have shown that R_0 for ilmenite is initially 4% but decreases down to 2.1% after 100 redox cycles with hydrogen as fuel gas.

Ilmenite's true density has been measured to 4580 kg/m^3 for *fresh* particles [68] using helium pycnometry. As helium penetrates even the finest pores, this method also considers the internal structure of the particles, i.e. it excludes the pores. With that in mind, "particle density", or "effective particle density", will from now on be referred to as the density of the particle including the pores. Eqs. (2.5)–(2.6) show the the relations between particle density (ρ_p), true density (ρ_t) and bulk density (ρ_b) as

$$\rho_p = (1 - \varphi)\rho_t \tag{2.5}$$

$$\rho_b = (1 - \epsilon)\rho_p. \tag{2.6}$$

Here, the variables φ and ϵ denote the porosity of the particle and the voidage of the bed, respectively. For fresh ilmenite, $\varphi = 0$ [68], i.e. $\rho_p = \rho_t$, while $\rho_b = 2370 \pm 120$ kg/m^3 depending on if the bed is loosely packed or more densely packed. From this, $\epsilon \approx 0.48$ for a normally packed bed of fresh ilmenite. After a number of cycles, when the particles have become activated, there is a significant decrease in the particle density as compared to the fresh case.

The question now comes to the *activated* ilmenite's particle density. During activation, the sphericity of the particles is increased due to rounding effects. Thus, it is likely that the voidage decreases when going from fresh to activated particles and ends up between the fresh case and the ideal case of uniformly sized spherical particles, i.e. $0.37 \leq \epsilon \leq 0.48$. Using a measuring jug and a scale, the bulk density of activated ilmenite has been found to lie in the range of 1170–2050 kg/m^3 [9, 69, 70]. Assuming $\epsilon = 0.43$, Eq. (2.6) yields instead a range in the activated particle density as $2050 \leq \rho_p \leq 3600$ kg/m^3, averaging at 2825 kg/m^3. Using instead He pycnometry and Hg intrusion techniques, Adánez et al. [68] measured the true density to 4250 kg/m^3 and porosity to 0.35 for activated ilmenite. Eq. (2.5) can then be used to calculate $\rho_p = 2760$ kg/m^3. This value of the activated ilmenite's particle density is the one used in Paper II. Table 2.1 summarises the findings using these methods and their respective sources. It is observed that there

Table 2.1: Different methods in determining the particle density of activated ilmenite.

ρ_b (kg/m^3)	ρ_t (kg/m^3)	ϵ (-)	φ (-)	ρ_p (kg/m^3)	Fuel	Source
1170–1750	n/a	0.43	n/a	2050–3070	Natural gas	[69]
2050	n/a	0.43	n/a	3600	Bit. coal	[9]
1200–1600	n/a	0.43	n/a	2100–2810	Syngas	[70]
n/a	4250	n/a	0.35	2760	$CH_4/H_2/CO$	[68]

is a significant variation in the particle density from particles activated under different conditions. Density decrease seems to be higher using gaseous fuels.

In a recent study [71], ilmenite has been shown to exhibit CLOU properties, see Section 1.3.7. This is relevant to chemical-looping combustion as it releases gas phase oxygen at the low oxygen partial pressure present in the fuel reactor. However, this O_2 release was found to be small, approximately 0.1% in the gas passing through the reactor beds. Table 2.2 presents some important characteristics of the ilmenite used in Papers I and III–VI. Values for sphericity, ϕ, were established from SEM images, the minimum fluidisation and terminal velocities (u_{mf},u_t) were calculated according to relations from Kunii and Levenspiel [72] for a density of 3.60 g/cm^3. The average particle diameter, $\bar{d}_p$, was calculated from the particle size distribution. Experimental values for R_0, BET and crushing strength are taken from [9].

Table 2.2: Characteristics of the activated oxygen carrier.

Property	Value
Reduced/oxidised form	$FeTiO_3/Fe_2TiO_5$+TiO_2
Average particle diameter, $\bar{d}_p$	171 μm
Sphericity, ϕ	0.7
Effective particle density, ρ_p	3.60 g/cm^3
Terminal velocity, u_t: air, 1000°C	0.83 m/s
Terminal velocity, u_t: steam, 950°C	0.91 m/s
Min. fluidisation velocity, u_{mf}: steam, 950°C	0.02 m/s
Theoretical (Experimental) R_0	5.0% (3.9%)
Specific surface area, BET	0.11 m^2/g
Crushing strength (fresh particles)	3.85 N

2.2 Setup of the 10 kW system (Paper I)

The 10 kW chemical-looping combustor [32] consists of an air reactor, connected to a loop seal on the inlet and outlet side, a fuel reactor and a smaller fuel reactor loop. It has two cyclones, one after the air reactor, where oxygen depleted air leaves the system, and one in the fuel reactor loop, where unreacted combustibles, combustion products and fluidisation gases leave the system. A sketch of the unit is shown in Fig. 2.1. The fuel reactor is divided into the following sections:

- LOVEL is the largest section and contains the majority of the bed material. For batch feeding, the fuel is fed through an external valve above the upper loop seal (not indicated in Fig. 2.1). Each batch, typically around 25 g, then drops down on top of the right-hand bed in LOVEL in a small clingfilm package. LOVEL is fluidised with steam.
- HIVEL is a small section below the riser, serving as outlet for the gases from the fuel reactor. This section is fluidised with inert nitrogen.

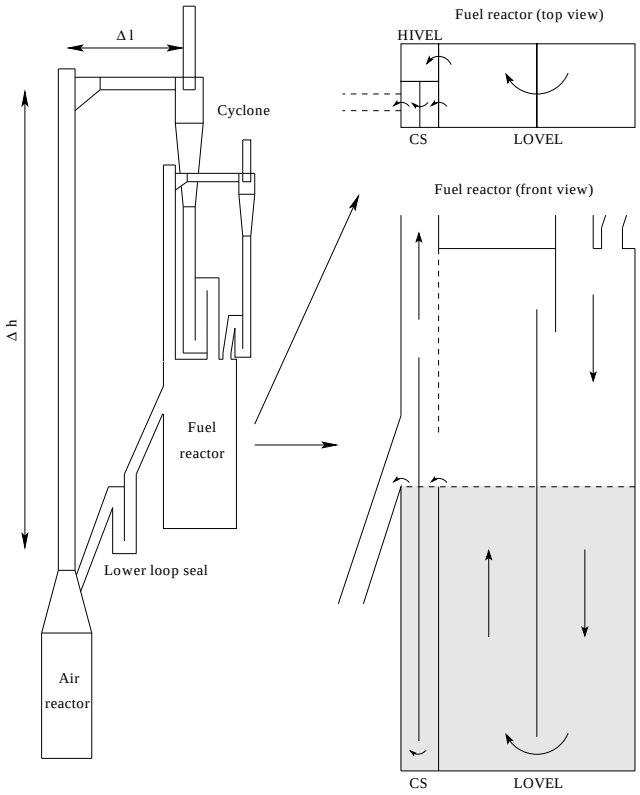

Fig. 2.1: Principle sketch of the 10 kW unit including a top and front view of the fuel reactor.

- CS is the carbon stripper, whose purpose is to elutriate unreacted char from the particle flow prior to its entrance into the air reactor. CS is also fluidised with N_2.

If the section is fluidised with nitrogen, reaction (1.4) can not occur. With the lower loop seal also fluidised with nitrogen, LOVEL is the section with essentially all syngas production.

2.3 Setup of the 100 kW system (Papers II–VI)

2.3.1 Reactor layout

During the initial planning of the 100 kW chemical-looping combustor, several configurations were discussed. The criteria that in the end led to the final design were:

- The air reactor riser should control the global circulation.
- The fuel reactor should be a circulating fluidised bed.
- A special riser for returning material to the air reactor is needed in order to keep the total height of the reactor system down.
- A carbon stripper should be implemented after the fuel reactor.
- The operation should be flexible, enabling both large variation in global solids circulation, fuel reactor bed height and fuel reactor fluidisation velocity.
- The system should be stable in operation and run little risk of loss in solids inventory in any part of the system.

The system includes two interconnected circulating fluidised beds, i.e. the air and the fuel reactor, as well as a carbon stripper. Starting in the fuel reactor, the path of solids circulation is outlined below and is numbered from 1–28 in Fig. 2.2. Gas and particles entrained in the fuel reactor (FR) enter the cyclone (CY2), fall down the downcomer to a loop seal (LS2) and enter the fuel reactor again. Particles not entrained may instead enter the so-called circulation riser (CR), which is placed in between the carbon stripper (CS1-4) and the loop seal (LS3) connected to the fuel reactor. The circulation riser is designed to return varying mass flows of particles to the air reactor. The carbon stripper has four chambers separated by weirs. The purpose of the carbon stripper is to gasify or separate residual char in the particle flow. The particles in the carbon stripper are passed on to a loop seal (LS4), leading to the air reactor (AR). The air reactor will re-oxidise the oxygen carriers before they are transported back to the fuel reactor by passing a cyclone (CY1) and another loop seal (LS1), beginning a new cycle. The air and fuel reactors are separated by loop seals in order to avoid gas mixing. Fig. 2.2 also shows how the different parts are interconnected. As seen in the sketch, it is the fuel reactor, with an inner height of 5.0 m, that determines the overall height of the unit.

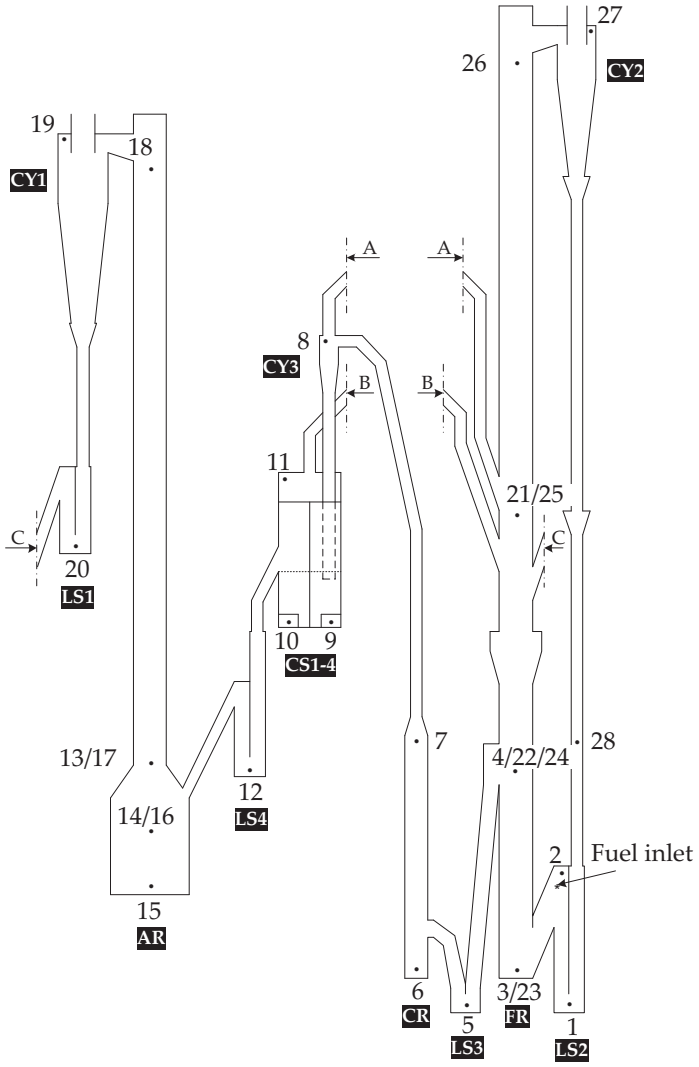

Fig. 2.2: A 2D sketch of the 100 kW unit.

2.3.2 The carbon stripper

As conversion of char is slow, chemical-looping combustors fed with solid fuels may incorporate carbon strippers. The main purpose of the carbon stripper is to separate unreacted char from the bed material and return it to the fuel reactor. Secondly, if the carbon stripper is fluidised with steam or CO_2, char conversion also occurs. With this dual function of the stripper, it is important to ensure sufficient residence time for the unseparated char in the bed. Fig. 2.3 shows the carbon stripper in the 100 kW unit, which employs four chambers, separated by weirs. This prevents the char from bypassing the bed by floating

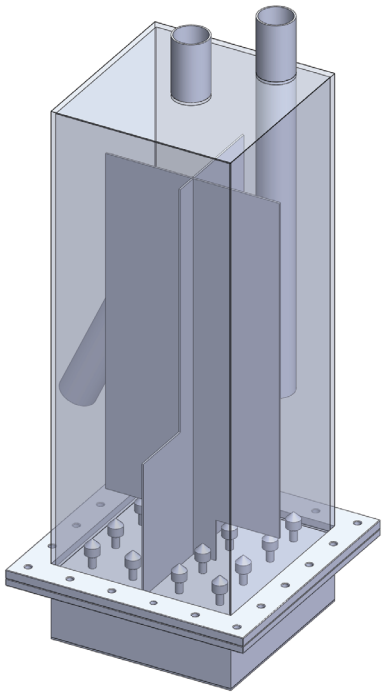

Fig. 2.3: Close-up of the four-chambered carbon stripper in the 100 kW unit.

on the surface and exit on the other side. As seen in Fig. 2.3, the bed material first enters the stripper though the pipe in the first chamber (CS1). This pipe goes down slightly below the surface of the bed. The particles then enter the second chamber (CS2) from underneath a separating wall. To enter the third chamber (CS3), the particles continue above another wall. Finally, the particles again need to go below a wall to enter the fourth chamber (CS4). Here, particles exit the stripper via an overflow exit and enter LS4. At the top of the stripper there is a common outlet for gases and entrained char particles, leading back to the fuel reactor. Every chamber in the stripper has four bubble caps, each with eight 1.5 mm holes fluidising the beds.

2.3.3 The cold-flow model

As discussed in Section 1.3.6, the key in designing a scale model is to identify the set of dimensionless parameters that successfully describe the physical processes of the full-scale system. This can be done by using Buckingham's π-theorem as a scheme for non-dimensionalisation of the governing equations [55]. For fluidised beds, a *full* and a *simplified* set of scaling laws have been derived, each consisting of a special set of so-called

π-groups. The π-groups, or scaling laws, are dimensionless combinations of the dimensionfull parameters that describe the physical process. The simplified set of scaling laws allows for an arbitrary scale to be chosen. However, some assumptions have been made regarding the flow regimes that might make it less accurate compared to the full set of scaling laws. Using the full set of scaling laws, the scale of the model will be determined by

$$f_{scale} \equiv \frac{D_{cold}}{D_{hot}} = \left(\frac{(\mu_f/\rho_f)_{cold}}{(\mu_f/\rho_f)_{hot}} \right)^{2/3}. \tag{2.7}$$

I.e., the scale is determined by the dynamic viscosity (μ_f) and density (ρ_f) of the fluidisation media in the two systems. The full set of scaling laws consists of the π-groups

$$\mathrm{Fr}, \frac{\rho_p}{\rho_f}, \mathrm{Re}_{d_p}, \mathrm{Re}_D, \frac{G_s}{\rho_p u_0}, \frac{L}{D}, \phi, \mathrm{PSD}, \tag{2.8}$$

where Fr is the Froude number, Re_{d_p} is the Reynolds number based on particle diameter, Re_D is the Reynolds number based on bed diameter, u_0 is the superficial velocity, D is the bed diameter, ρ_p is the particle density, ρ_f is the fluidisation gas density, G_s is the particle flux, L is a bed-related length (e.g. height), ϕ is the particle sphericity and PSD is the particle size distribution. Choosing to use the same density particles in the hot and cold-flow model, i.e. $(\rho_p)_{cold} = (\rho_p)_{hot}$, the cold-flow model fluidisation gas must have the same density at ambient temperature (20℃) as steam at 950℃. The only gas that would be possible for this task is helium. Thus, using helium in room temperature, i.e. $(\rho_f)_{cold} = (\rho_f)_{hot}$, yields $f_{scale} = 0.5766 \approx 58\%$. This is an acceptable size, hence the construction of the cold-flow model was determined to follow the full set of scaling laws. The requirements for dynamic similarity between the systems are summarised in Table 2.3.

Table 2.3: Atmospheric chemical-looping combustor with corresponding ideal cold-flow model.

Given	CLC unit	Ideal CFM
Temperature (℃)	950	20
Gas viscosity (μPas)	45.03	19.72
Particle density (g/cm^3)	~ 2.76	~ 2.76
From scaling laws		
Gas density	$(\rho_f)_{hot}$	$(\rho_f)_{hot}$
Diameters or lengths	D_{hot}	$0.577 D_{hot}$
Particle diameter	$(d_p)_{hot}$	$0.577 (d_p)_{hot}$
Superficial velocity	$(u_0)_{hot}$	$0.759 (u_0)_{hot}$
Volumetric particle flux	$(G_s/\rho_p)_{hot}$	$0.759 (G_s/\rho_p)_{hot}$
Time	t_{hot}	$0.759 t_{hot}$

There are different options for selecting bed material to use in the cold-flow model. One is to extract activated particles from the hot unit, then crush and sieve them until a sufficient amount is obtained. A second is to use other particles with the same density, sphericity and PSD as the activated ilmenite particles. For convenience, a fine silica sand

(GA39) provided by Sibelco Nordic, consisting of 98.8% SiO_2, was chosen as bed material. Its average particle diameter, $\bar{d}_p = 92$ μm, is close to the ideal case ($0.577 \cdot 171 = 99$ μm). It will have approximately the same sphericity ($\phi \approx 0.75$) but a more narrow PSD than the ilmenite. The largest uncertainty is the particle density of the activated ilmenite. Following the discussion in Section 2.1, based on the jug/scale method of measurement, the activated ilmenite is expected to have a particle density between 2050–3600 kg/m^3 whereas the value derived from He pycnometry was 2760 kg/m^3. The silica sand has a particle density of 2650 kg/m^3, which, with the given uncertainty, should be adequate to describe the system in accordance with the prerequisite $(\rho_p)_{cold} = (\rho_p)_{hot}$. A 3D sketch of the 100 kW system is shown in Fig. 2.4(a) and the cold-flow model itself, with supporting scaffold, is shown in Fig. 2.4(b).

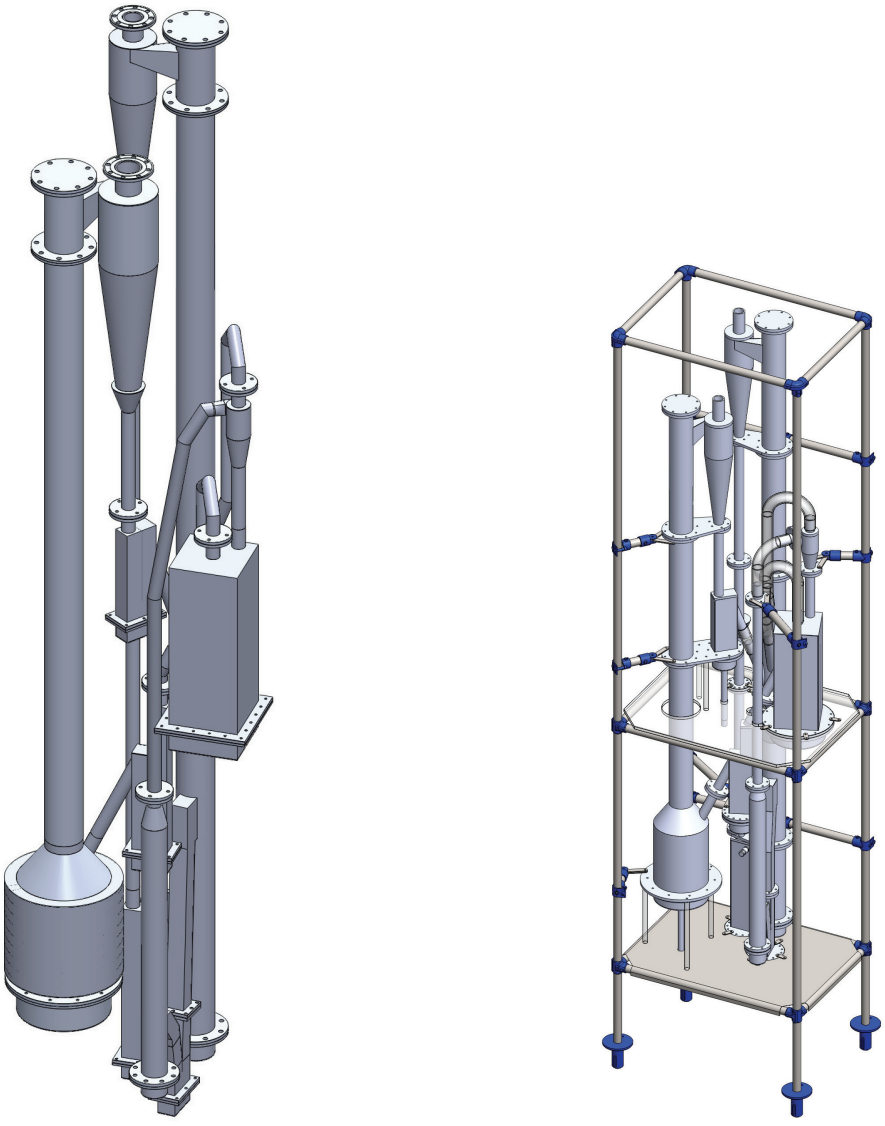

(a) (b)

Fig. 2.4: (a) The designed 100 kW reactor system and (b) the lab-scale cold-flow model with supporting scaffold. The cold-flow model is approximately 58% the size of the 100 kW unit.

2.3.4 Fuel

Three fuels have been tested in the 100 kW unit. A Colombian bituminous coal (LHV = 29.12 MJ/kg, $\bar{d}_p$ = 105.2 μm), a Mexican petroleum coke (LHV = 31.75 MJ/kg, $\bar{d}_p$ = 79.0 μm) and another coal from Colombia: Cerrejón coal (LHV = 24.64 MJ/kg, $\bar{d}_p$ = 42.9 μm). Table 2.4 shows the composition and Table 2.5 the PSD of the fuels. It can be noted that the Cerrejón coal particles have a much smaller size than the other two.

Table 2.4: Composition of the different fuels.

Content	Colombian coal (%)	Mexican petcoke (%)	Cerrejón coal (%)	Comment
C-fix	54.53	81.54	48.2	as received
Volatiles	37.04	10.00	29.4	as received
Moisture	3.25	8.00	13.8	as received
Ash	5.18	0.46	8.6	as received
C	80.78	88.84	84.30	moisture and ash free
H	5.41	3.14	5.90	moisture and ash free
O	11.59	0.49	7.38	moisture and ash free
N	1.54	0.96	1.65	moisture and ash free
S	0.69	6.58	0.77	moisture and ash free

Table 2.5: Particle size distribution of the different fuels.

Size (μm)	Colombian coal (wt-%)	Mexican petcoke (wt-%)	Cerrejón coal (wt-%)
< 45	6.5	14.9	52.0
45-90	20.4	28.9	36.0
90-125	17.4	15.4	8.0
125-180	21.9	19.9	4.0
180-212	12.4	10.0	-
212-250	13.4	9.0	-
> 250	8.0	2.0	-

2.3.5 Fuel feeding

This 100 kW unit is designed for use with a pulverised fuel that can be fed through a set of screws. The unit employs two screws, where the first controls the overall feeding rate of the fuel while the other transports the fuel into the reactor system. The internals and the outside of the second screw are cooled with three separate streams of water. Fuel is fed into the reactor together with a nitrogen sweep-gas. The feeding point of the fuel is

located on top of the bed in loop seal LS2, see Fig. 2.2. Following the solids flow, the fuel is then transported into the lower part of the bed in the fuel reactor. Thus, this method of feeding the fuel can effectively be regarded as in-bed fuel feeding. As the fuel enters the hot reactor, volatiles will immediately be released, causing a large volume expansion. To avoid gas production from char gasification in the downcomer from the cyclone (CY2), loop seal LS2 is fluidised with nitrogen instead of steam. The process of char gasification starts in the neighbouring fuel reactor and continues all the way to loop seal LS4. However, as soot may form on the walls above the bed in LS2, a steam flow called "LS2 Fuel" may be inserted from the ceiling of LS2. The experiments conducted in Paper III–IV employed a 16 L fuel container, enabling storage of around 8 kg of fuel with a bulk density of 0.5 g/cm^3. In Paper V, the experiments were conducted using a 300 L fuel container. Using a fuel with the same bulk density as mentioned above, this container enables operation for 10 hours using a feeding rate of 15 kg/h (100 kW fuel power).

2.3.6 Fluidisation and mass distribution

In Table 2.6, data on the fluidisation are summarised. It provides the fluidisation gas in the different parts as well as mass flow intervals commonly used. The bottom part cross-section area for each section is also provided. Here, the cross-sections of CR, FR and AR are circular, CS is square and the loop seals rectangular (1:2). The mass flows do not include the contribution from fuel devolatilisation and gasification. The last column shows the approximate mass distribution of bed material at a standard flow setting. Typical bed inventories in the entire unit lies between 220–280 kg.

Table 2.6: Mass flows, bottom part cross-section areas (A_c) and mass distribution of particles in the unit. The mass flows are the flows through the windboxes and are provided in the range within which they are most often varied. The cross-section of the narrow air reactor riser is the same as in the fuel reactor.

Section	Gas	Flow (kg/h)	A_c (cm^2)	Mass (%)
LS1	H_2O	1.5-2	115	2.2
LS2 Fuel	H_2O	0-1	115	-
LS3	H_2O	1.5-2	115	7.2
LS4	H_2O	1.5-2	115	3.1
CS1	H_2O	3-4	225	5.7
CS2	H_2O	3-4	225	5.7
CS3	H_2O	3-4	225	5.7
CS4	H_2O	3-4	225	5.7
CR	H_2O	5-10	82	4.0
FR	H_2O	5-15	186	16.3
LS2	N_2	2.3	115	6.3
AR	Air	128.8-194.0	1257	38.3
Fuel screw	N_2	2.3-4.5	0.85	-
Total	H_2O	26.5-48.0	-	-
Total	N_2	4.5-6.8	-	-

2.3.7 Temperature, pressure and gas measurements

There are more than 60 pressure taps all over the system where pressure is measured. These pressure taps are not only placed on the 100 kW unit itself, but also on the air cooling pipes, in order to estimate the flow velocity, and in the filter connected to the sedimentation tank/heat exchanger loop, in order to get an indication on when it is full and needs to be changed. Temperature is also measured in several places, both in the reactor and in the peripheral equipment, such as in the steam generator system, the steam pipes, the scrubber, the sedimentation tank and several places along the flue gas outlet pipes. Fig. 2.5 shows 49 of the pressure tap locations as well as 6 positions (T1–T6) where temperature is also measured. The gas analyser that measures concentrations

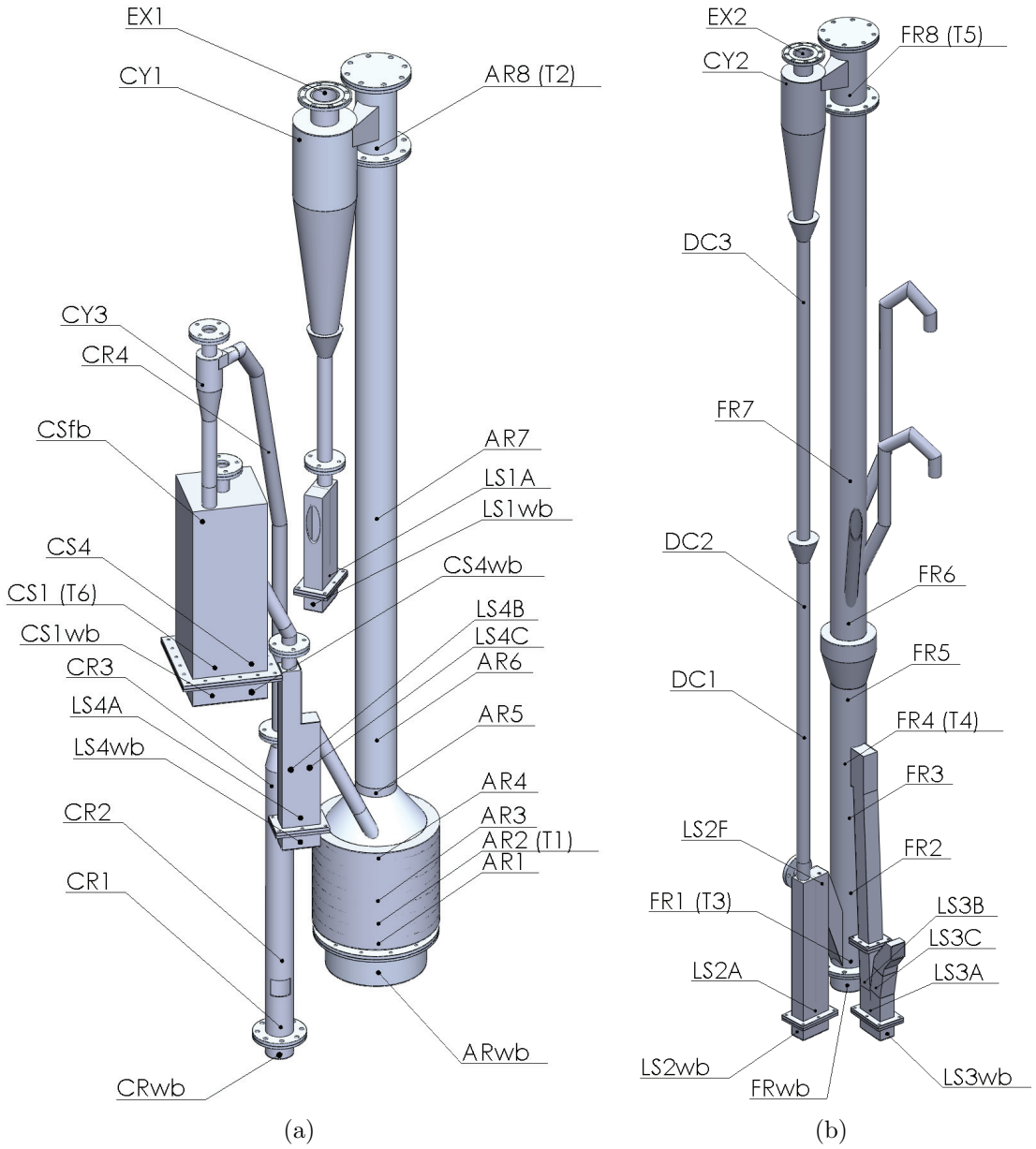

Fig. 2.5: Split-up drawings of Fig. 2.4(a), cut between LS3 and CR, with section labels referring to Fig. 2.2. Here, (a): CR, CS, LS4, AR, CY1 and LS1, while (b): CY2, LS2, FR and LS3.

from the fuel reactor is an Emerson Rosemount NGA 2000, while the analyser measuring concentrations from the air reactor is a Sick Maihak S710. The analyser measuring the NO concentration from the fuel reactor is an Emerson XStream.

2.4 Data evaluation (Papers I–VI)

2.4.1 Measurements of circulation in a riser

The upward mass flux of particles in a riser can be estimated from [73] as

$$G_s = \frac{1}{g}\frac{\Delta P_{\Delta h}}{\Delta h}(u_0 - u_t), \tag{2.9}$$

where g is the gravitational acceleration, Δh a small distance at the top of the riser over which a pressure $\Delta P_{\Delta h}$ is measured, u_0 the superficial velocity and u_t the terminal velocity of a particle. This estimate appears in Papers I, II and IV, but is used in all papers when analysing the upward mass flux of particles in a riser. The mass flow derived from Eq. (2.9) is $A_c \cdot G_s$, where A_c is the cross-section area of the riser. In Paper I, it is called $\dot{m}_{G_s}$, while in Papers II and IV it is called $\dot{m}_{riser}$. This mass flow is different from the mass flow that actually passes through to the cyclone. This is due to the fact that some upward moving particles will hit the ceiling of the riser and fall down again along the walls. Hence, the (estimated) riser mass flow overestimates the (actual) circulation mass flow, $\dot{m}$. The ratio $\dot{m}/\dot{m}_{G_s}$ or $\dot{m}/\dot{m}_{riser}$ will from here on be referred to as the *flow-through ratio*. Inspired by Eq. (2.9), another measure of the circulation was used by Berguerand and Lyngfelt [32]. This measure is called the circulation index, CI, where

$$CI = \Delta P_{\Delta h+\Delta l} \cdot F_{AR,out}. \tag{2.10}$$

Here, $\Delta P_{\Delta h+\Delta l}$ is the pressure drop measured between pressure taps located at the riser bottom and at the cyclone inlet, directly after the riser exit, cf. Fig. 2.1, and $F_{AR,out}$ is the volume flow of gas in the air reactor at the current temperature. This relation is used in Paper I as a measure of the circulation rate in the 10 kW unit.

2.4.2 Oxygen demand

The oxygen demand, Ω_{OD}, is the fraction of oxygen lacking to achieve a complete combustion of the gases leaving the fuel reactor. The gas conversion, γ, is given from the oxygen demand as $1 - \Omega_{OD}$. The oxygen demand is calculated as

$$\Omega_{OD} = \frac{0.5x_{CO,FR} + 2x_{CH_4,FR} + 0.5x_{H_2,FR} + 1.5x_{H_2S,FR}}{\Phi_0(x_{CO_2,FR} + x_{CO,FR} + x_{CH_4,FR})}, \tag{2.11}$$

where Φ_0 is the oxygen/carbon ratio, i.e. the ratio of moles of oxygen needed to convert the fuel completely per moles of carbon in the fuel, and $x_{i,FR}$ is the molar fraction of species i in the gas from the fuel reactor. Here, an estimation of H_2S was only available and accounted for in the tests using Cerrejón coal. For the first Colombian coal and the Mexican petroleum coke, $x_{H_2S,FR}$ was set to zero. This gives a small underestimation in

the oxygen demand, especially for the sulphur-rich petroleum coke. The concentration of H_2S was not measured, but calculated from the measured concentration of SO_2 as

$$x_{H_2S,FR} = (x_{CO_2,FR} + x_{CO,FR} + x_{CH_4,FR}) \times \frac{S}{C} - x_{SO_2,FR}, \tag{2.12}$$

where the sulphur-to-carbon ratio, S/C, is calculated on molar basis from the coal analysis. Thus, it is assumed that the sulphur-to-carbon ratio is the same in gaseous phase as in solid phase. However, it is possible that some SO_2 is dissolved in condensate water, leading to an overestimation of the H_2S concentration. For the first Colombian coal: $\Phi_0 = 1.149$, for the Mexican petroleum coke: $\Phi_0 = 1.138$ and for the Cerrejón coal: $\Phi_0 = 1.179$.

2.4.3 CO_2 capture efficiency

There are two common ways to measure the efficiency of CO_2 capture in solid fuel chemical-looping combustion. They are the calculation of the carbon capture, η_{CC}, and oxide oxygen, η_{OO}, efficiencies.

The carbon capture efficiency for continuous fuel feeding is defined as the ratio of the carbon containing gas flow, leaving the fuel reactor, to the total carbon containing gas flow leaving the air and fuel reactors. It can be calculated as

$$\eta_{CC} = \frac{x_{CO_2,FR} + x_{CO,FR} + x_{CH_4,FR}}{\frac{F_{AR}}{F_{FR}} x_{CO_2,AR} + x_{CO_2,FR} + x_{CO,FR} + x_{CO_4,FR}}, \tag{2.13}$$

where F_{AR} and F_{FR} are the total, dry, gas flows in the air and fuel reactors, respectively. F_{AR} is known, while F_{FR} is calculated from knowledge of the total nitrogen flow, $F_{N_2,FR}$, in the fuel reactor as

$$F_{FR} = \frac{F_{N_2,FR}}{x_{N_2,FR}}, \tag{2.14}$$

where the nitrogen composition (on dry basis), $x_{N_2,FR}$, is estimated from

$$x_{N_2,FR} = 1 - x_{CO,FR} - x_{CO_2,FR} - x_{CH_4,FR} - x_{H_2,FR}. \tag{2.15}$$

The oxide oxygen efficiency is defined as the amount of oxygen used for oxidising the particles in the air reactor, divided by the total amount of oxygen consumed in the air reactor. It only depends on the gas concentrations in the air reactor outlet, eliminating any uncertainty due to flows. It is calculated as

$$\eta_{OO} = \frac{0.21 - x_{O_2,AR} - x_{CO_2,AR}}{0.21 - x_{O_2,AR} - 0.21 x_{CO_2,AR}}. \tag{2.16}$$

The oxygen needed for char combustion in the air reactor yields an oxygen-to-carbon ratio, O_2/C, of one. The oxygen needed for oxidation of the fuel yields a somewhat higher oxygen-to-carbon ratio, c.f. Φ_0 for the different fuels. However, because of the incomplete oxidation in the fuel reactor, O_2/C is close to one. Thus, the numerator will represent the carbon released as gas in the fuel reactor, whereas the denominator will represent the total carbon released. Therefore, the definition used will give a good representation of the efficiency with which CO_2 is captured.

The calculation of the carbon capture efficiency might be less accurate than the oxide oxygen efficiency due to the dependency of the flows. With this in mind, the oxide oxygen efficiency is hereby referred to as *the CO_2 capture efficiency*. Paper I uses η_{CC} to measure the capture efficiency, while Paper III–V use η_{OO}.

3

Modelling

3.1 Residence-time analysis (Paper I)

3.1.1 Mass-flow from residence time

The residence-time is a basic variable in any study of a combustion unit with fluidised beds. For example, assume that the mass flow of particles cannot be measured directly. Then the mass flow needs to be determined by some other means. If the residence-time and bed mass are known, then the mass flow could be calculated from the definition of the residence-time as

$$\dot{m} = \frac{m}{\tau}. \tag{3.1}$$

The aim of Paper I was to investigate the residence-time distribution of circulating bed material in a 10 kW chemical-looping combustor for solid fuels.

3.1.2 The multistage-bed model

Inspired by [74], the derivation of the multistage-bed model is sketched below. First, assume that there is a fluid passing through a series of N continuous stirred-tank reactors (CSTRs). Let V_k denote the volume of the k:th CSTR (m^3) and Q the overall volume flow (m^3/s). After the k:th CSTR, let $\dot{n}_k$ denote the molar flow (mol/s) and C_k the concentration (mol/m^3) of a substance in the fluid. The aim of this analysis is to find the time dependent concentration of the substance after the last CSTR. A molar balance over the k:th CSTR can be written

$$\dot{n}_k = \dot{n}_{k-1} - dn_k/dt, \tag{3.2}$$

where dn/dt refers to the molar rate of change. If the molar change is $dn_k = V_k dC_k$ and molar flow $\dot{n}_k = QC_k$, then Eq. (3.2) can be written

$$QC_k = QC_{k-1} - V_k \frac{dC_k}{dt}. \tag{3.3}$$

Dividing with Q on both sides and recognising that $\tau_k = V_k/Q$ then yields

$$C_k(t) = C_{k-1}(t) - \tau_k \frac{d}{dt} C_k(t). \tag{3.4}$$

This differential equation can be solved using Laplace transforms. A Laplace transform of Eq. (3.4) would *effectively* change $d/dt \rightarrow s$ and $C_k(t) \rightarrow \widetilde{C}_k(s)$. Treating the time derivative as a parameter s, Eq. (3.4) can be transformed to

$$\frac{\widetilde{C}_k(s)}{\widetilde{C}_{k-1}(s)} = \frac{1}{1+\tau_k s}. \tag{3.5}$$

Assuming that the volume of each reactor is equally large, i.e. $\tau_k = \tau/N$, where τ is the total residence-time, means that Eq. (3.5) is the same for all CSTRs. Hence

$$\frac{\widetilde{C}_N}{\widetilde{C}_0} = \frac{\widetilde{C}_N}{\widetilde{C}_{N-1}} \cdot \frac{\widetilde{C}_{N-1}}{\widetilde{C}_{N-2}} \cdot \ldots \cdot \frac{\widetilde{C}_1}{\widetilde{C}_0} = \left(\frac{1}{1+\tau s/N}\right)^N. \tag{3.6}$$

Defining the last expression as $\widetilde{H}(s)$ yields $\widetilde{C}_N(s) = \widetilde{H}(s)\widetilde{C}_0(s)$. The inverse Laplace transform of a product becomes an integral, hence

$$C_N(t) = \int_{t'=0}^{t} H(t')C_0(t-t')dt, \tag{3.7}$$

where $H(t)$ and $C_0(t)$ are the individual inverse transforms of $\widetilde{H}(s)$ and $\widetilde{C}_0(s)$, respectively. If the substance is released at time $t = 0$, then $C_0(t) = C_0\delta(t)$, where C_0 is a constant. Eq. (3.7) then simplifies to

$$C_N(t) = C_0 H(t), \tag{3.8}$$

where $H(t)$ is found in standard mathematical tables to be

$$H(t) = \frac{1}{(N-1)!}\left(\frac{N}{\tau}\right) t^{N-1} e^{-t/(\tau/N)}. \tag{3.9}$$

The time dependence of the concentration after the N:th CSTR is thus

$$C_N(t) \sim t^{N-1} e^{-t/(\tau/N)}. \tag{3.10}$$

When feeding the fuel reactor with a batch of fuel, the char content will gasify and gradually reduce the oxygen carrier. This will effectively create a batch of reduced oxygen carriers that eventually will enter the air reactor. This batch can be viewed as a batch of oxygen with negative concentration. With the bed material acting as the fluid and the batch of oxygen with negative concentration acting as the added substance, Eq. (3.10) can be correlated to measured concentrations in the 10 kW unit. It is assumed that the fuel reactor and lower loop seal can be modelled as a series of N equally sized CSTRs. When the batch of reduced oxygen carriers reach the air reactor, the oxygen concentration will decrease. If the model is successful, then the oxygen concentration should be possible to fit

$$x_{O_2,AR}(0) - x_{O_2,AR}(t) \sim t^{N-1} e^{-t/(\tau/N)}. \tag{3.11}$$

3.1.3 Data sampling and experimental conditions

The experiments were conducted with batch loading of the fuel. To reduce the risk of fuel particles sticking to the walls, the batches were released in the fuel reactor in small

packages made by clingfilm. The clingfilm mass was negligible and did not affect the experiments when converted in the bed. The mass of the batches was varied, but typically sets of 25 g were used. Mexican petroleum coke, with a total volatile fraction of close to 10%, was used in testing with several modes of circulation and two different temperatures. As the batches were released into the fuel reactor, a time frame of around 40 seconds was noted until the gas analysers registered any change. Data was saved for around 20–25 minutes before ending each trial as at that time no noticeable concentrations were observed. The gas analyser Sick Maihak S710 was used for selective analysis of IR-absorbing gases for the CO, CO_2 and CH_4 measurements and the paramagnetic principle for the O_2 measurements.

3.1.4 Correlation to measured data

The experimental data used in the model is obtained with Mexican petroleum coke, fed in batches for different circulations at 950℃ and 970℃. By varying the circulation index, see Eq. (2.10), while measuring the oxygen concentration in the air reactor, it is possible to correlate the coefficients in Eq. (3.11) to the measured data. With N as input, the residence-time is found using a least squares fit. See Fig. 3.1 for the correlation at $CI = 141$ kPa·L/min. Here, the light-gray data is excluded from the fit as it is assumed to be a "dead-volume tail". The "dead-volume tail" is a phenomenon caused by the corners and right angles in the reactor sections, where fluidisation can locally be deficient. This means that a time delay, not represented in the model, is introduced. The time delay will

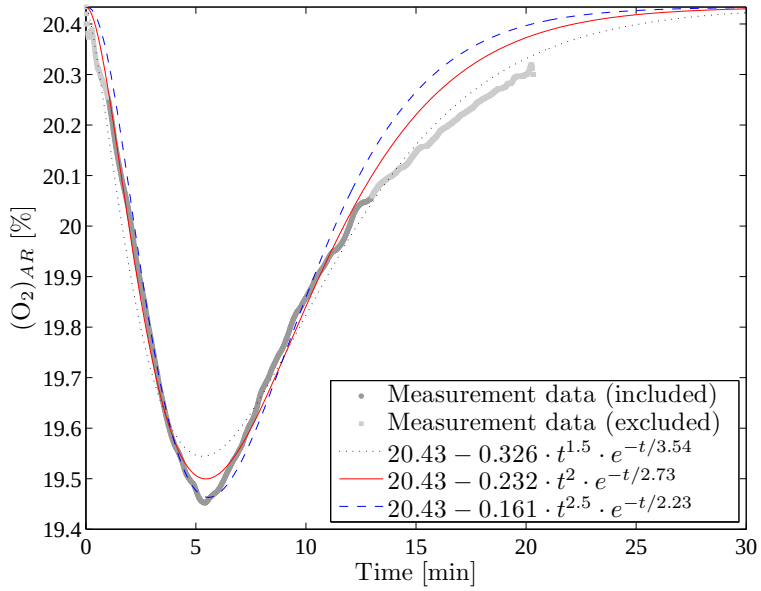

Fig. 3.1: $CI = 141$. The three lines here correspond to $N = 2.5$, $N = 3$ and $N = 3.5$, where $\tau = 8.2$ min is found for $N = 3$. The fuel-reactor temperature was 950℃.

induce a weaker slope of the oxygen concentration in the air reactor at the final minutes. Fig. 3.1 also shows how N is chosen. For this example, three alternatives for N are studied: 2.5, 3 and 3.5. $N = 2.5$ produces a curve with too low amplitude, while $N = 3.5$ drops off too steep. Hence, the middle alternative $N = 3$ was chosen. The results for all CI are

Table 3.1: Results of the residence-time analysis.

CI [kPa·L/min]	34	78	102	121	141	256
N [-]	1.8	2.0	2.5	3.0	3.0	3.0
τ [min]	35.5	14.3	11.0	9.6	8.2	5.7

shown in Table 3.1. As this analysis was done for several different CI, it was possible to correlate the residence-time to the circulation index. The correlation found was

$$\tau = \frac{1178 \pm 58}{CI}, \tag{3.12}$$

with a 95% confidence bound, see Fig. 3.2. Eqs. (3.1) and (3.12) then yield a relation to the mass flow as

$$\dot{m} = \frac{m_\tau}{1178} \cdot CI. \tag{3.13}$$

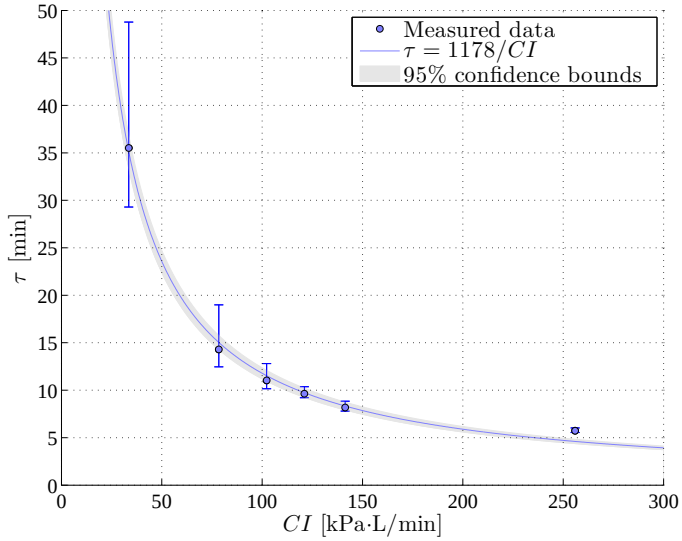

Fig. 3.2: Measured data and least-squares fit of the residence-time versus circulation index for 950℃ and 970℃. The data points are accompanied by error bars corresponding to the lower and upper limits (dashed and dotted, respectively) for the different choices of N.

3.1.5 The flow-through ratio

As discussed in Section 2.4.1, the circulation mass flow is smaller than the riser mass flow. Exactly how much smaller is partly dependent on e.g. the shape of the cyclone entrance and the fluidisation velocity. Using $\dot{m}$ as the label for the circulation mass flow, as calculated from the residence-time model results, and $\dot{m}_{G_s}$ as the riser mass flow from Eq. (2.9), a plot as in Fig. 3.3 can be produced. It shows that the circulation mass flow from the air reactor is approximately 22% of the riser mass flow, for the lower circulation

indices. Here, the last point has been excluded from the fit, hence for $\dot{m} > 1$ kg/min it is likely that the flow-through ratio, $\dot{m}/\dot{m}_{G_s}$, is less than 22%.

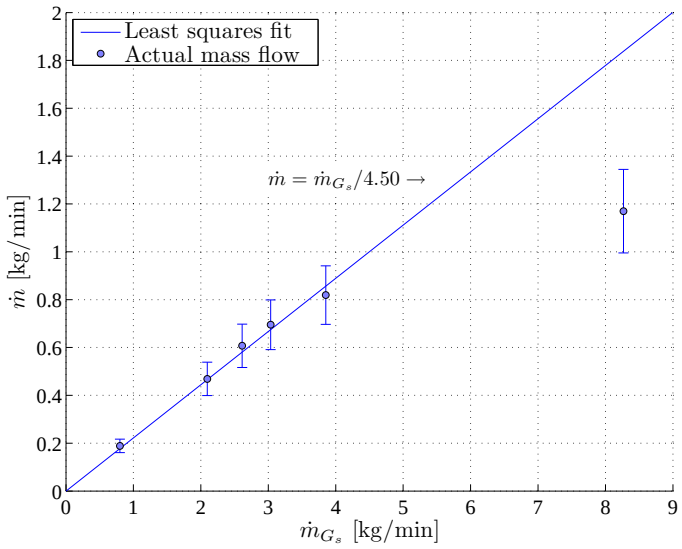

Fig. 3.3: The circulation mass flow $\dot{m}$, determined from the residence-time, versus $\dot{m}_{G_s}$, determined from the mass flux of Eq. (2.9).

3.2 The cold-flow model (Paper II)

3.2.1 Data sampling and experimental conditions

The most interesting parameters in cold-flow model measurements are the pressures, the particle mass flows and the gas volume flows. The pressures are measured using over 30 pressure transmitters from Huba Control. Gas flows are controlled by 8 El-Flow Base/Select models from Bronkhorst. Mass flows of bed material are manually measured by aid of three butterfly valves, integrated in the cold-flow model. Each valve is placed after a cyclone, hence there is one after CY1, CY2 and CY3, respectively, see Fig. 2.2. Pressure data are read and stored every 1/10 seconds for at least 3 minutes in stable operation before averaging. Particle mass flows are measured 10 times in stable operation giving an average value. It is done by aid of a soft ruler, pasted above the butterfly valve, and a stopwatch. The errorbars presented in Figs. 3.6 and 3.7 are defined by $\pm$ one standard deviation from these 10 measurements.

3.2.2 Slug-analysis in the circulation riser

Slugging is common is tall, narrow beds of solids. The most critical part concerning slugging in the cold-flow model is the circulation riser. Observations during operation in a default fluidisation setting confirm that there indeed is slugging in this section. Fluidising with ambient air, the bed material, having average particle diameter $\bar{d}_p = 92$ μm and particle density $\rho_p = 2.65$ g/cm^3, are between Geldart A and B solids, hence the slugs formed are a mixture of axial slugs and wall slugs [72]. Fluidisation in the circulation riser

was investigated for four different fluidisation velocities, varying from 0.21–0.57 m/s, see Fig. 3.4. It shows the pressure drop between two points in the upper part of the riser, above the bed. This figure also includes information on the mean value μ, the standard deviation

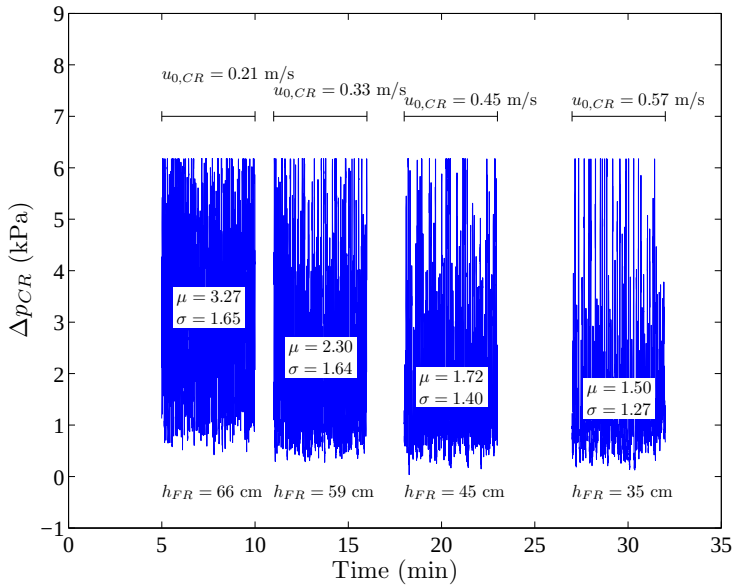

Fig. 3.4: Pressure difference between two points in the top of the circulation riser.

σ, and the current bed height in the fuel reactor h_{FR}. The bed height was measured with a ruler after quickly having shut off the fluidisation flows. As can be observed, the peaks are cut at roughly 6 kPa. This is a limitation in the pressure transmitter installed between these two points. However, it is possible to see a trend with more fluctuations for the lower velocities and less fluctuations for the higher velocities. This has to do with the terminal velocity of the sand particles, u_t, which is close to 0.41 m/s with ambient air. Hence, when passing this limit, the transfer of particles will not only occur with slugs, but also with a continuous flow. This decreases the pressure fluctuations. On the other hand, the bed height in the fuel reactor falls considerably when $u_{0,CR} > u_t$. The bed height in FR should be at least 59–60 cm, i.e. the height to the overflow exit to LS3, hence $u_{0,CR} = 0.33$ m/s was chosen as default velocity in the circulation riser.

3.2.3 Bed inventory stability

If no changes are made to the flow in the circulation riser, i.e. $u_{0,CR} = 0.33$ m/s, then an increase in either the air or the fuel reactor flow may rearrange the bed inventories by transferring particles from the fuel reactor to the air reactor or vice versa. Evidence of this is shown in Fig. 3.5. For example, increasing the fluidisation velocity in the air reactor will increase the circulation mass flow and decrease its bed mass slightly. At the same time, the bed mass in the fuel reactor will increase slightly. Experiments show that, after a change, a new steady state is assumed. This means that if the outgoing mass flow is increased by a certain amount, the incoming mass flow will also increase with the same amount. For the chosen $u_{0,CR}$, it is evident from Fig. 3.5 that the circulation mass flow, both in the fuel reactor loop and between the air and fuel reactor, can be varied in a wide range with only minor changes in solids inventory.

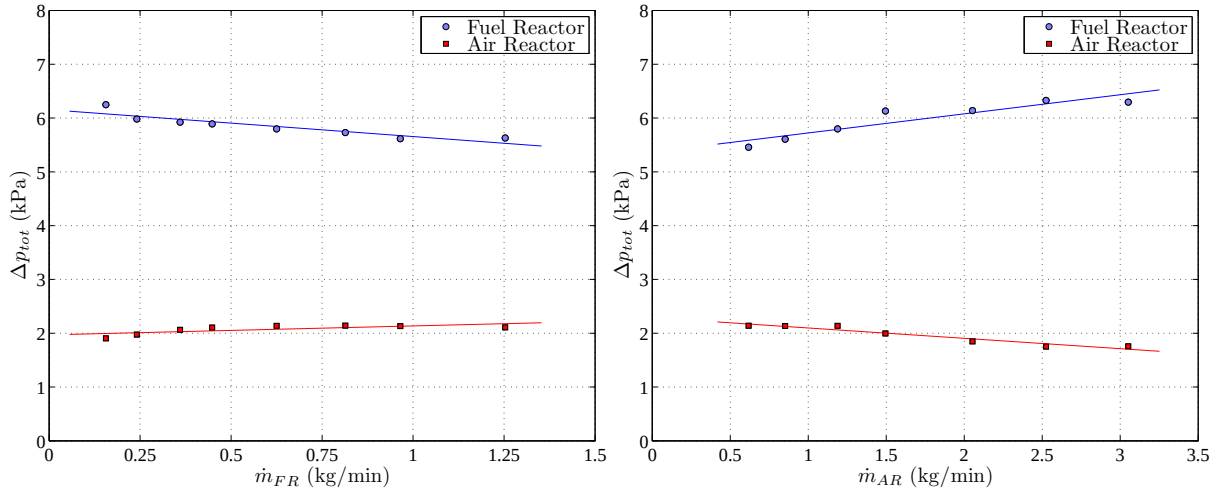

(a) Varying $\dot{m}_{FR}$ through the FR gas velocity.

(b) Varying $\dot{m}_{AR}$ through the AR gas velocity.

Fig. 3.5: Pressure difference over the whole fuel and air reactor as function of circulation mass flows. Here, $\dot{m}_{FR}$ is the circulation mass flow of the internal FR loop, while $\dot{m}_{AR}$ is the circulation mass flow of the major AR–FR loop.

3.2.4 The flow-through ratio

Similar to the analysis in Section 3.1.5, the flow-through ratios ($\dot{m}/\dot{m}_{riser}$) for both the fuel and air reactors in the cold-flow model are measured. The riser mass flow, $\dot{m}_{riser}$, is calculated from Eq. (2.9) using the pressure difference between points 17–18 in Fig. 2.2, i.e. the pressure difference between points AR5 and AR8 in Fig. 2.5(a). The circulation mass flow, $\dot{m}$, is measured with the butterfly valve implemented in the downcomer after each respective cyclone. The results are shown in Fig. 3.6. The circulation mass flow was found to be 45% of the riser mass flow for the fuel reactor and 29% for the air reactor.

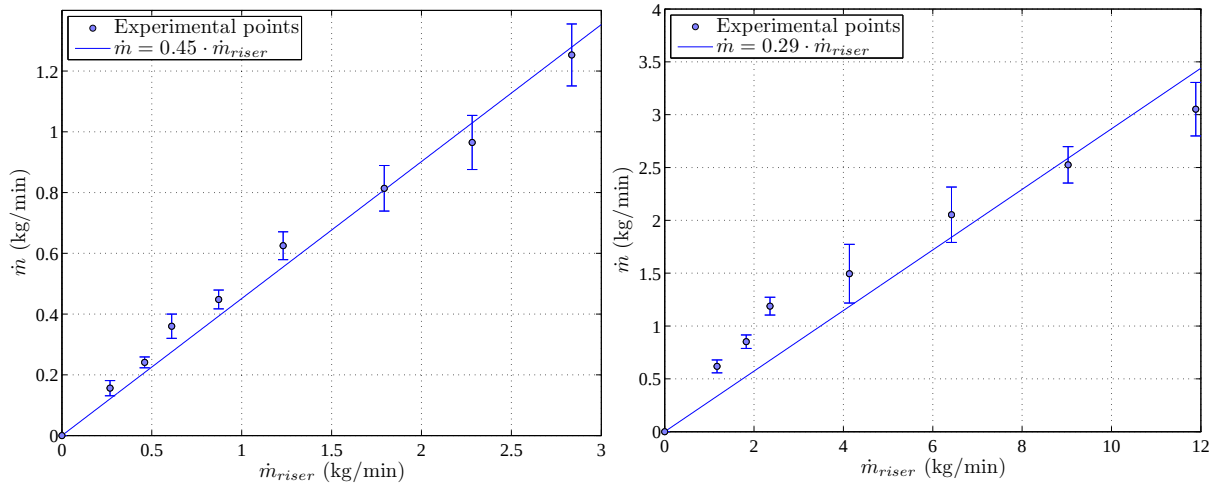

(a) The fuel reactor.

(b) The air reactor.

Fig. 3.6: The circulation mass flow entering the cyclone versus the riser mass flow.

3.2.5 Residence-time

With knowledge of the bed mass in different parts of the system, the residence-time can be calculated from Eq. (3.1). E.g. for the air reactor, the mass flow is the global solids circulation as measured by the butterfly valve in the cyclone downcomer. Fig. 3.7 shows the residence time in the air reactor for different superficial velocities. Here, $\tau_{AR} = m_{AR}/\dot{m}_{AR}$ is the average residence-time of a particle in the air reactor

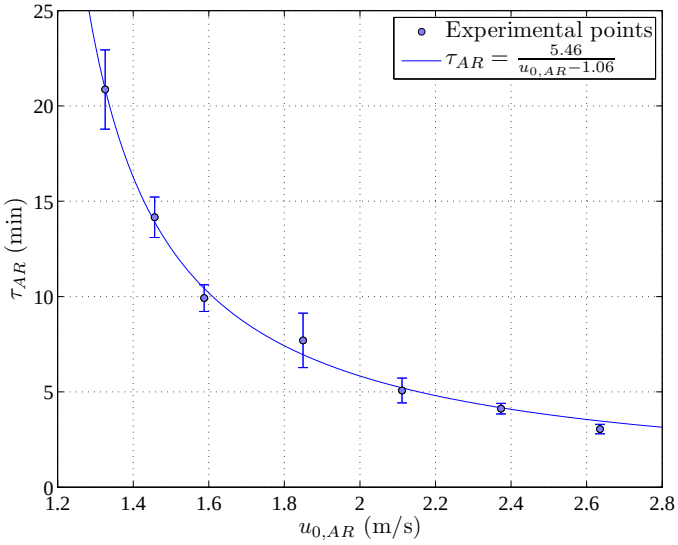

Fig. 3.7: The residence-time versus the superficial velocity in the air reactor.

3.3 Modelling gas conversion (Paper VI)

In the 100 kW unit, fuel is fed on top of the bed in the loop seal next to the fuel reactor, see Section 2.3.5. Immediately, devolatilisation of the fuel starts, releasing CO, H_2, CH_4 as well as other hydrocarbonaceous gases. However, as this loop seal is fluidised with nitrogen, steam gasification is negligible. Not until the fuel has reached the fuel reactor, the gasification process of the char begins according to reaction (1.4), producing syngas. Two dimensionless quantities are introduced, κ and α, defined as

$$\kappa \equiv \frac{F_g}{F_0} \tag{3.14}$$

$$\alpha_i \equiv \frac{k_{F,i} m}{F_0}, \tag{3.15}$$

where F_g is the total flow of gas above the bed (converted and unconverted) from the gasification and devolatilisation of the fuel, F_0 is the fluidisation flow of steam, $k_{F,i}$ is the mass-based reaction rate constant between the oxygen carrier and an unconverted species i, and $\dot{m}$ is the total bed mass. Assuming that the bed has an even distribution of char particles with no volatiles present, the model predicts that the partial pressure of species i (CO or H_2) is given by

$$p_i(\alpha) = \frac{p_{i,max}}{\alpha_i + \kappa} \left[(1+\kappa) - (1+\kappa)^{-\alpha_i/\kappa} \right], \tag{3.16}$$

where $p_{i,max}$ is the maximum partial pressure of species i. In the other extreme, assuming that there is no char present and that volatiles enter at the bottom of the bed, the model predicts that the partial pressure of species i (CO, H_2 or CH_4) is given by

$$p_i(\alpha) = p_{i,max} \cdot e^{-\alpha_i}. \tag{3.17}$$

As the model treats each unconverted gas species separately, an individual gas conversion component can be defined for each species as

$$\gamma_{CO} = \frac{p_{CO_2}}{p_{CO} + p_{CO_2}} \tag{3.18}$$

$$\gamma_{H_2} = \frac{p_{H_2O}}{p_{H_2} + p_{H_2O}} \tag{3.19}$$

$$\gamma_{CH_4} = \frac{p_{CO_2}}{p_{CH_4} + p_{CO_2}} \tag{3.20}$$

This means that $\gamma_i(\alpha) = 1 - p_i(\alpha)/p_{i,max}$ for both Eq. (3.16) and Eq. (3.17), yielding

$$\gamma_{c,i}(\alpha) = 1 - \frac{(1+\kappa) - (1+\kappa)^{-\alpha_i/\kappa}}{\alpha_i + \kappa} \tag{3.21}$$

$$\gamma_{v,i}(\alpha) = 1 - e^{-\alpha_i} \tag{3.22}$$

for species i of the char conversion (c) and volatiles conversion (v), respectively. Fig. 3.8 shows Eq. (3.21) for $\kappa > 0$. From this plot, it can be observed that $\gamma_{c,i}$ is practically

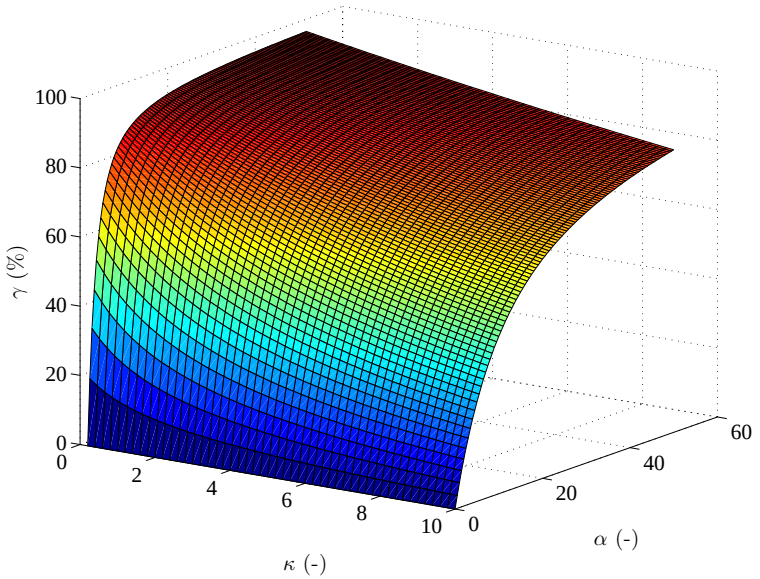

Fig. 3.8: Illustration of $\gamma_{c,i}$'s dependence on κ and α according to Eq. (3.21).

independent of κ for $0 < \kappa < 1$ if $\kappa \ll \alpha$. For these conditions, a good approximation of Eq. (3.21) is

$$\gamma_{c,i} \approx 1 - \frac{1}{\alpha_i}, \tag{3.23}$$

with an error less than 1% if $\alpha \gtrsim 4$.

During real fluidisation, some unconverted gas bypass the bed through bubbles and avoid contact with the oxygen carrier. As the model does not consider these facts, a correction can be added. Defining $\phi_{s,core}$ as the fraction of solids exposed to the gas passing in plug flow [75], α would change to

$$\alpha_\phi = \phi_{s,core}\alpha. \tag{3.24}$$

As the parameter α contains the bed mass, it is reasonable that $\phi_{s,core}$ enters here. The correction $\phi_{s,core}$ may take different values for Eqs. (3.21) and (3.22) as it is likely that the contact between gas from char gasification and bed material differs from that of volatiles and bed material.

In order to find an expression for the total gas conversion with respect to char and volatiles, each component needs to be weighted with respect to the oxygen consumption for full conversion of the species. In the case of CO and H_2 for char conversion, the weights would be 50% each, i.e. gas conversion for char is calculated as

$$\gamma_c = 0.5\gamma_{c,CO} + 0.5\gamma_{c,H_2}. \tag{3.25}$$

For the volatiles, data from [76] provide the gas composition for a typical bituminous coal in rapid pyrolysis. From this data, the gas conversion for volatiles was estimated as

$$\gamma_v = 0.079\gamma_{v,CO} + 0.290\gamma_{v,H_2} + 0.632\gamma_{v,CH_4}. \tag{3.26}$$

Finally, Eqs. (3.25) and (3.26) need to be weighted together to form an overall gas conversion for the fuel. From a fuel analysis of the Cerrejón coal, see Table 2.4, assuming no loss of char to the filters, it is possible to show that the overall gas conversion can be calculated as

$$\gamma = 0.624\gamma_c + 0.376\gamma_v. \tag{3.27}$$

A correction for the fraction of char, lost from the system, should be added to the model. To this end, defining ξ as the fraction of char that is converted, i.e. *not* lost, γ in Eq. (3.27) would change to

$$\gamma_\phi = 0.624\xi\gamma_c + (1 - 0.624\xi)\gamma_v. \tag{3.28}$$

Here, the subscript ϕ refers to the correction to γ, made by $\phi_{s,core}$ and ξ.

Instead of regarding γ_ϕ as a function of α, it can be noted that the bed mass is related to the pressure drop according to

$$m = \frac{A_c}{g}\Delta p. \tag{3.29}$$

Hence, gas conversion can effectively be modelled as a function of the fuel reactor pressure drop, Δp.

4

Operation

The operational periods presented in Paper III–V consist of over 23 hours of operation with fuel in the 100 kW unit. In this chapter, three representative operational periods were selected for presentation. The periods are the first operation with Colombian coal (Co-I), the operation with Mexican petroleum coke (M-I) and seventh operation with Cerrejón coal (Ce-VII). All data are sampled at a rate of 1 Hz. In the plots showing the oxygen demand and CO_2 capture efficiency, a floating average of 10 seconds has been applied in order to filter out some of the noise. The measured concentrations do not add up to 100%. This is mainly due to dilution with nitrogen, originating from the fuel screw, LS2 and minute quantities from the pressure tap sweep gas. All concentrations are measured on dry gas and are corrected for minor in-leakage of air on the way to the analysers. In some figures, small gaps in the data exist during a few minutes throughout the operational period. These gaps indicate when the sample gas pipes are flushed with nitrogen in order to clean them from steam condensate. The mass flow of particles, $\dot{m}$, was approximated from batch experiments as described in Section 4.3. The air reactor temperature was controlled using a mantle cooler, through which ambient air exchanges heat with the hot wall of the air reactor. Temperatures presented from the air and fuel reactors are measured at points T1 and T3, see Fig. 2.5, respectively. In Appendix A, a comprehensive list with startup and shutdown procedures for operation of the 100 kW system is provided.

4.1 Operation with Colombian coal (Paper III)

For the first operational period with Colombian coal in the 100 kW unit, fuel was fed for 70 minutes at 6.9 kg/h. The gas concentrations from the fuel reactor are shown in Fig. 4.1. Note that CO_2 is diluted by N_2 fluidising LS2 and N_2 entering with the fuel screw and pressure taps. As fuel is introduced at $t = 0$ min, a drop in the fuel reactor temperature of approximately 5℃ can be observed, see Fig. 4.2(a). Approximately 3.5 min later, the temperature starts to rise in the air reactor as reduced oxygen carrier particles reach the air reactor. After some additional time, the fuel reactor temperature is regained as warmer particles from the air reactor return. During the last 30 min of operation with fuel, the average temperature was 948℃ in the fuel reactor and 992℃ in the air reactor. Fig. 4.2(a) shows that it is possible to operate the unit under stable temperature

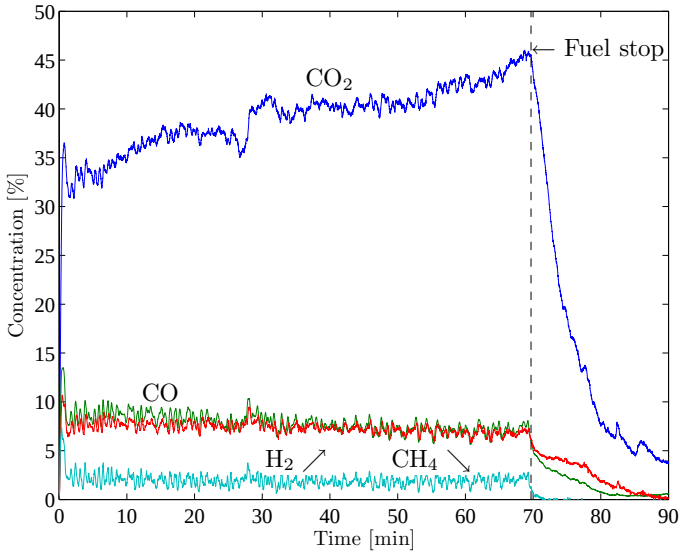

Fig. 4.1: Flue gas concentrations from the first operational period with the Colombian coal.

conditions. Conversion to CO_2 increases as the ilmenite is gradually activated and as char accumulates and the fraction of gases coming from volatiles decrease, see Fig. 4.2(b). Thus, the oxygen demand drops from approximately 25% to 18.5%, which is the average

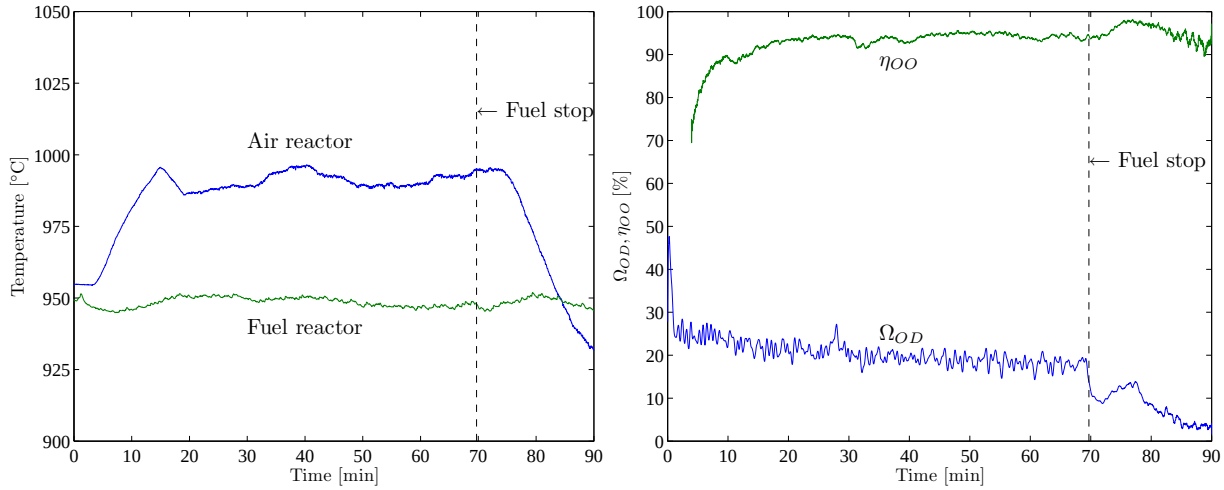

(a) Temperatures in the air and fuel reactor.

(b) CO_2 capture and oxygen demand.

Fig. 4.2: Temperatures in the air and fuel reactor as well as CO_2 capture efficiency (η_{OO}) and oxygen demand (Ω_{OD}) from the first operational period with the Colombian coal.

from the last 30 minutes. The average CO_2 capture from the last 30 minutes was 94.4%. These data can be compared to results from the 10 kW unit, where the oxygen demand obtained was around 23% and the CO_2 capture $\sim$ 90% at 970°C in the fuel reactor with the same coal, although partially devolatilised, and oxygen carrier [9]. As fuel addition stops, oxygen demand drops significantly. This is a result of volatiles not being released any more, and indicates that the oxygen demand for char conversion is significantly lower.

4.2 Operation with Mexican petroleum coke (Paper IV)

For the operational period with the Mexican petroleum coke, fuel was fed during 32 minutes at 11.3 kg/h. Compared to operation with the Colombian bituminous coal, the gas concentration curves are smoother, see Fig. 4.3. The smoothness most likely depends

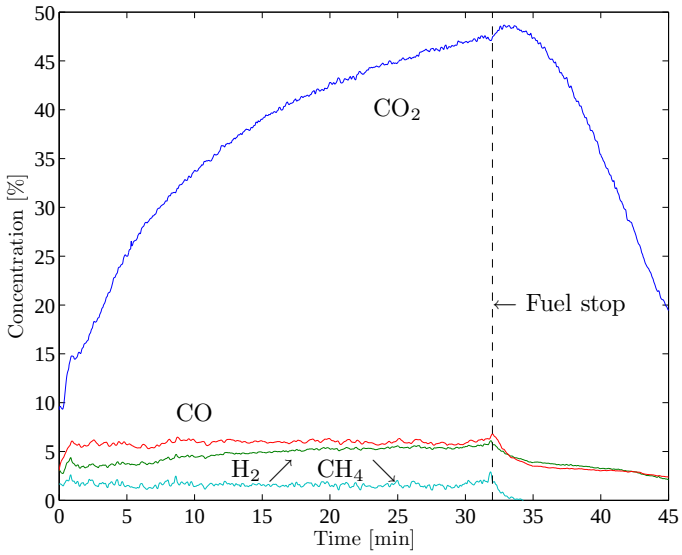

Fig. 4.3: Flue gas concentrations from the operational period with the Mexican petroleum coke.

on the low volatile content, see Table 2.4. Fig. 4.4(a) shows the temperatures in the air and fuel reactor. No stable temperature was achieved in the air reactor during the

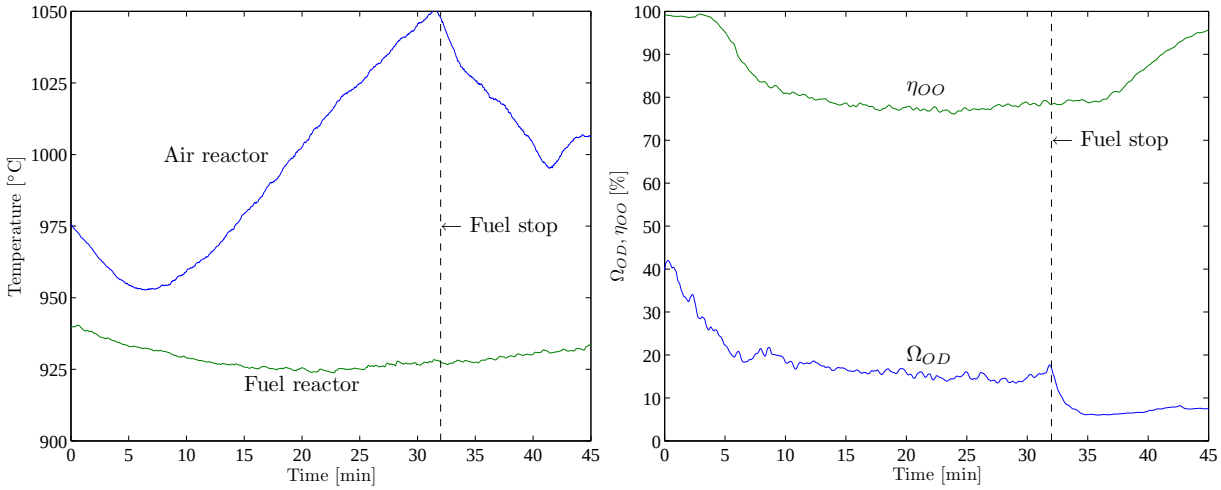

(a) Temperatures in the air and fuel reactor.

(b) CO_2 capture and oxygen demand.

Fig. 4.4: Temperatures in the air and fuel reactor as well as CO_2 capture efficiency (η_{OO}) and oxygen demand (Ω_{OD}) from the operational period with the Mexican petroleum coke.

period of fuel feeding. The temperature was as high as 1050°C in the air reactor and no operational difficulties were noted. However, the average temperatures during the last 10

minutes were 1033℃ in the air reactor and 926℃ in the fuel reactor. The average oxygen demand from the last 10 minutes was 14.8%, while the average CO_2 capture efficiency was 77.7%, see Fig. 4.4(b). The low oxygen demand can be explained by the low volatile content of the fuel. This can be compared with the observation that the oxygen demand goes down when the fuel feeding stops, i.e. when the volatiles disappear. The low CO_2 capture efficiency is due to the high fraction of char in the fuel. A higher fraction of char means that longer residence times and higher temperatures may be needed to obtain an efficient CO_2 capture. Again, comparing to results obtained in the 10 kW unit with the same fuel and oxygen carrier at 970℃ in the fuel reactor [9], an oxygen demand of 18–21% and a CO_2 capture of 60–70% were found.

4.3 Measuring circulation in the 100 kW unit (Paper IV)

The mass flow of particles can be approximated from batch experiments. Here, a batch of ~ 330 g of Cerrejón coal was fed during 1 minute at 20 kg/h. Using the method outlined in Section 3.1.4 (Paper I), the residence time was calculated to 7.3 minutes at the current settings. It was assumed that the system of chambers from the point of fuel insertion till the entry of the air reactor, with a total bed mass m_τ, can be modelled as a plug flow reactor (PFR) in series with a set of continuous stirred-tank reactors (CSTRs). The time it took from fuel start till the first indication of an O_2 dip in the air reactor provided the residence time in the plug flow section, while an analysis of the O_2 dip itself (see Paper IV) provided the residence time in the CSTRs. Thus it was found that,

$$\tau = \tau_{PFR} + \tau_{CSTR} = 3.2 + 4.1 = 7.3 \text{ minutes}. \tag{4.1}$$

The total bed mass in the steam-fluidised sections between the fuel feed point and the entry to the air reactor is estimated to $m_\tau = 165$ kg. Eq. (3.1) then implies that $\dot{m} = m_\tau/\tau = 22.5$ kg/min. During this same period, the estimated riser flow was calculated from Eq. (2.9), i.e.

$$\dot{m}_{riser} = \frac{A_c}{g}\frac{\Delta p_{riser}}{\Delta h}(u_0 - u_t), \tag{4.2}$$

where $\dot{m}_{riser} = \dot{m}_{G_S}$ and $\Delta p_{riser} = \Delta P_{\Delta h}$. Here, the pressure drop was measured between the top of the air reactor riser and the closest pressure tap 1.6 metres below, i.e. between points AR7 and AR8 in Fig. 2.5(a). The average pressure drop during the batch experiment was 629 Pa, yielding an estimated riser flow of 277.8 kg/min. This results in a flow-through ratio of 8.09%. Hence, it is assumed that the mass flow through the cyclone CY1 is given by

$$\dot{m} = 0.081 \cdot \dot{m}_{riser} \tag{4.3}$$

for all experiments.

4.4 Operation with Cerrejón coal (Paper V)

The aim with the experiments using Cerrejón coal was to investigate the effect of key operational parameters on the system behaviour and thereby the performance. The system behaviour includes global solids circulation, distribution of solids between reactors and

operational stability of the system, whereas the performance indicators include gas conversion as well as CO_2 capture. From this study, it should be possible to find operational conditions that give high performance. The seventh operational period with Cerrejón coal provided 5.2 h of operation with fuel. Table 4.1 shows the parameter changes in events labelled from 1 to 10 in Figs. 4.5–4.8, where event 0 states the settings at $t = 0$ min. In

Table 4.1: Parameter changing events from the seventh operational period.

Event	AR flow (L_n/min)	FR flow (kg/h)	CR flow (kg/h)	Fuel flow (kg/h)	T_{AR} (°C)
0	1660	15	5	6.3	1000
1	1660	15	5	12.6	1000
2	2000	15	5	12.6	1000
3	2250	15	5	12.6	1000
4	2500	15	5	12.6	1000
5	2500	5	5	12.6	1000
6	2500	5	5	12.6	1025
7	2500	5	10	12.6	1025
8	2500	5	5	12.6	1025
9	2500	15	5	12.6	1025
10			Fuel stop		

Fig. 4.5, the concentrations of CO_2, CO, H_2, CH_4 and NO from the fuel reactor as well as O_2 and CO_2 from the air reactor are plotted. Here, the NO concentration is scaled up with

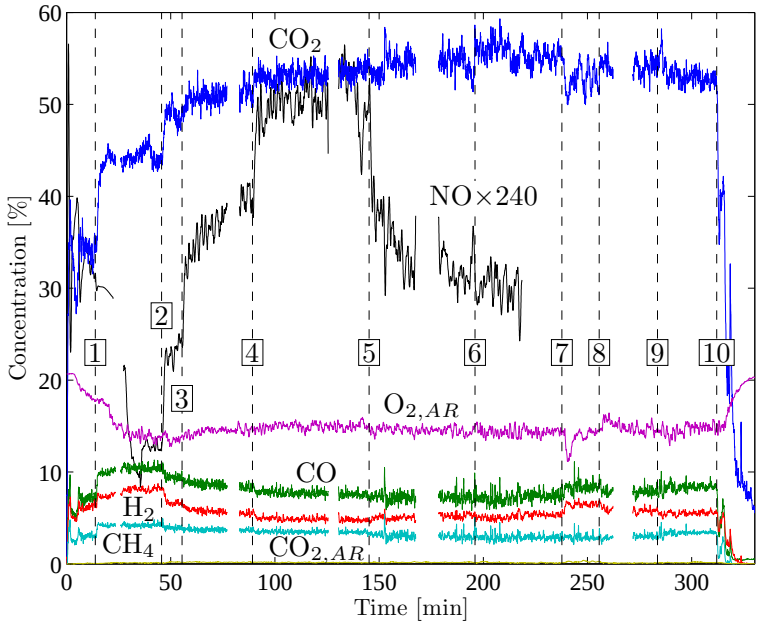

Fig. 4.5: Flue gas concentrations from the seventh operational period with the Cerrejón coal.

a factor of 240. This would mean that if $x_{NO} \times 240 = 30\%$, then $x_{NO} = 1250$ ppm. The

sulphur gas concentrations are not presented due to the uncertainty in the amounts solved in condensate water. At event 1, where the fuel feeding rate is increased, both the CO_2 as well as the unconverted gases can be seen to increase, as expected. However, as soon as the air reactor flow is increased, see events 2–4, the concentration of unconverted gases decreases, while the CO_2 and NO concentrations increase. This is also reflected in the significant reduction of the oxygen demand, see Fig. 4.6. As seen in Fig. 4.7, this is correlated

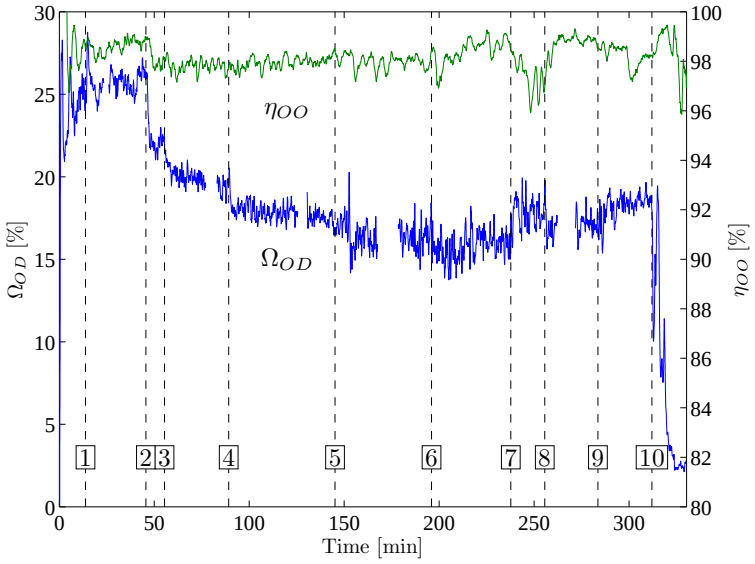

Fig. 4.6: CO_2 capture efficiency (η_{OO}) and oxygen demand (Ω_{OD}) from the seventh operational period with the Cerrejón coal.

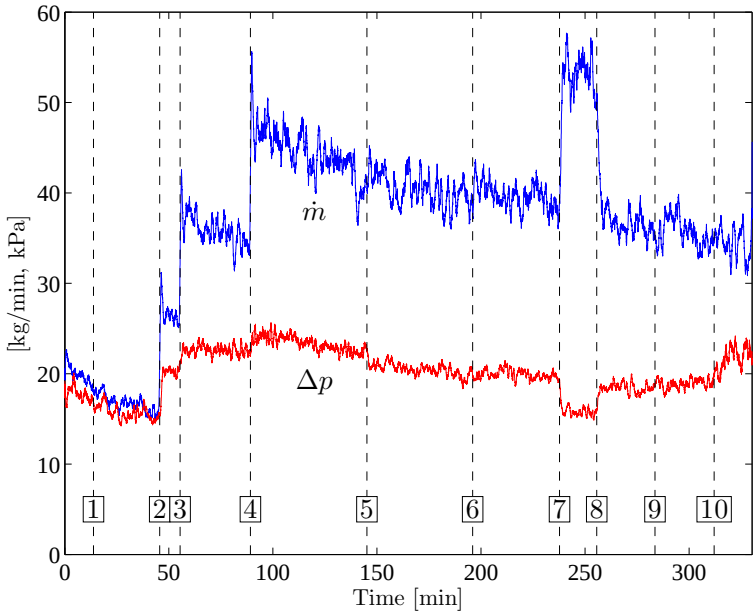

Fig. 4.7: Mass flow ($\dot{m}$) and total pressure drop in the whole fuel reactor (Δp) from the seventh operational period with the Cerrejón coal.

to the increased bed height in the fuel reactor. At event 5, when the fuel reactor flow is lowered from 15 to 5 kg/h, the NO concentration goes down rapidly at the same time as the oxygen demand decreases further. From Fig. 4.6 it is also seen that lowering the fuel reactor flow from 15 to 5 kg/h at event 5 does not seem to affect the CO_2 capture. Up to event 5, the fuel reactor temperature was fairly constant, see Fig. 4.8. However, when the fuel reactor flow was lowered from 15 to 5 kg/h, the temperature increased slightly. Next increase is seen to occur as the air reactor temperature was increased, providing hotter particles to the fuel reactor. The air reactor temperature was regulated to 1000℃ for the

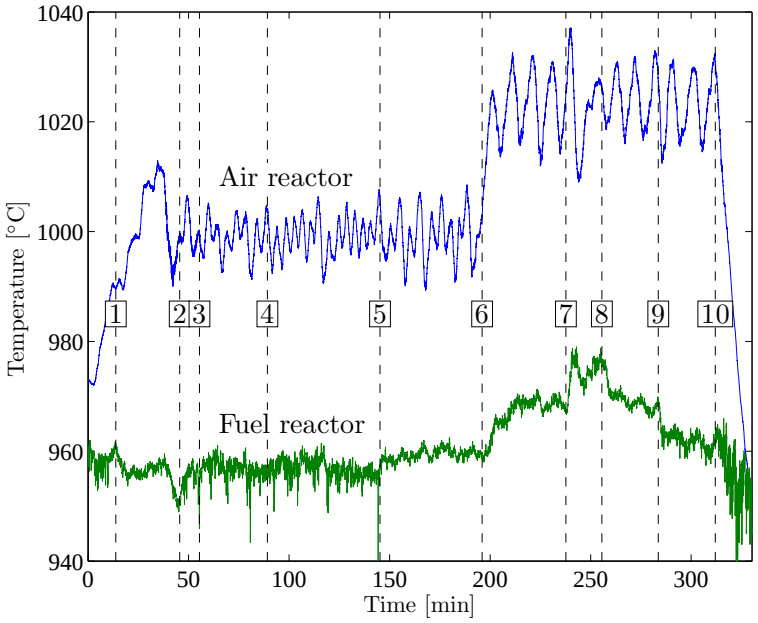

Fig. 4.8: Temperatures in the air and fuel reactor.

first $\sim$ 200 minutes, after which it was set to 1025℃ at event 6. The fuel reactor temperature during the experiment varied between 950–980℃. At event 6, when the fuel reactor temperature increases from approximately 960℃ to 970℃, the oxygen demand is lowered slightly, while the CO_2 capture is improved. Increasing the circulation riser flow from 5 to 10 kg/h at event 7 is shown to have a detrimental effect on both oxygen demand and CO_2 capture. It can also be seen that the circulation is rapidly increased. This increase resulted in a lowered bed inventory in the fuel reactor, see Fig. 4.7. At this point, the CO_2 concentration goes down while the CO and H_2 concentrations go up. At event 8, when the flow in the circulation riser is again set to 5 kg/h, the temperature also returns to its previous value. The same can be seen for both the circulation and the fuel reactor bed inventory. At event 9, a similar behaviour of the temperature is seen when the fuel reactor flow is returned from 5 kg/h to 15 kg/h.

To summarise, important changes were made to the AR flow, the FR flow, the CR flow and air reactor temperature. The resulting effects from these changes were:

- Increased AR flow lowers the oxygen demand and increases circulation and fuel reactor inventory. Furthermore, the NO concentration also increases.
- The oxygen demand goes down slightly when the FR flow is decreased. CO_2 capture seems largely unaffected. Interestingly, the increased gas conversion in this case is

not accompanied by increased NO concentration. Instead, NO drops drastically.

- The increase in CR flow led to a drastic increase in global solids circulation, a lowering of the fuel reactor bed inventory, a lower CO_2 capture and a higher oxygen demand.
- As the the fuel reactor temperature increases by 10°C, an improvement is shown in both gas conversion and CO_2 capture.
- No adverse effects of operating the air reactor at 1025°C for 2 h were detected.

4.5 Overview of operation

This thesis presents results from fourteen different operational periods, conducted in a 100 kW chemical-looping combustor for sold fuels using ilmenite oxygen carriers. Table 4.2 summarises the results, including the average gas concentrations, from a total of fourteen experiments. The last row shows the time period before fuel termination, Δt_{avg}, over which $\dot{m}$, Ω_{OD}, η_{OO}, T_{FR}, Δp and the gas concentrations were averaged, except for experiment Ce-IX where the average is taken between 165–200 min. A special case is Co-II, where the averages were taken during the final 10 minutes, except for η_{OO}, $x_{NO,FR}$ and the AR concentrations which were averaged for 2 minutes. The label "C-gas" in rows 9–11 is the sum of CO_2, CO and CH_4. Rows 9–11 are given in %.

Table 4.2: Summary of fourteen experiments in the 100 kW unit.

	Co I	Co II	Co III	M I	Ce I	Ce II	Ce III	Ce IV	Ce V	Ce VI	Ce VII	Ce VIII	Ce IX	Ce X
$\dot{m}$ (kg/min)	15.7	7.2	9.5	10.5	16.3	19.7	12.9	17.8	18.4	27.7	40.3	39.9	38.7	15.7
t_{fuel} (min)	70.0	28.8	42.0	32.0	22.0	17.7	20.0	13.4	8.4	144	312	85	245	351
$\dot{m}_{fuel}$ (kg/h)	6.9	11.5	4.9	11.3	18.5	20.3	20.3	29.8	?	19	12.6	12.6	12.6	12.6
Ω_{OD} (%)	18.5	24.0	21.2	14.8	19.6	19.4	25.7	24.5	22.2	21.6	16.9	15.9	16.3	16.7
η_{OO} (%)	94.4	92.3	96.0	77.7	91.3	74.9	88.4	86.2	87.1	96.4	98.2	97.1	98.3	99.5
T_{FR} (°C)	948	919	932	926	941	931	922	923	925	944	964	964	963	955
Δp (kPa)	14.9	12.4	12.3	10.8	15.4	20.2	12.3	13.1	13.6	15.2	19.5	22.7	19.7	22.7
$x_{CO_2,FR}$ (%)	41.8	31.8	42.7	45.8	52.3	30.0	44.1	53.8	51.7	47.4	54.2	54.8	54.9	53.2
$x_{CO}/x_{C\text{-}gas}$	14.2	19.1	16.6	10.3	14.0	12.8	16.5	14.9	13.5	14.1	11.7	11.1	11.0	10.9
$x_{H_2}/x_{C\text{-}gas}$	13.7	15.5	14.0	11.3	9.5	7.0	12.4	11.2	10.0	9.5	8.3	7.3	8.4	7.9
$x_{CH_4}/x_{C\text{-}gas}$	3.7	5.2	4.6	3.0	5.5	6.2	7.7	7.7	7.0	6.6	4.7	4.5	4.5	4.9
$x_{NO,FR}$ (ppm)	n/a	n/a	n/a	n/a	n/a	n/a	149	163	338	n/a	1290	930	1332	842
$x_{CO_2,AR}$ (%)	0.5	0.4	0.2	1.5	1.3	3.2	1.2	1.8	0.7	0.4	0.1	0.3	0.1	0.03
$x_{O_2,AR}$ (%)	14.5	17.3	17.3	15.4	8.4	10.5	12.4	10.4	16.7	12.2	14.5	13.4	14.5	16.2
Δt_{avg} (min)	30	10/2	10	10	5	5	5	5	5	10	180	30	35	20

4.6 Pressure profiles (Paper V)

From cold-flow model experiments, a pressure profile has been produced (Paper II). The pressure in any point of the fluidised reactor system relative to some reference pressure, e.g. the pressure at the top of the fuel reactor cyclone, depends on the amount of particles between the pressure taps and the effective voidage between the particles. This voidage depends on if the particles are in a dense phase, an entrained phase above the bed or in a splash zone between the other two phases. If Δh is the vertical distance to where

the reference pressure is measured, then $\Delta p_g \sim (1 - \epsilon_{eff})\rho_p \Delta h$, where Δp_g is the gauge pressure, ϵ_{eff} is the effective voidage between the particles up to the reference pressure and ρ_p is the particle density. If the effective voidage is assumed the same for the sand particles in the cold-flow model as for the ilmenite in the 100 kW unit, then the upscaled pressure drop from cold-flow model experiments is

$$\Delta p_{g,h} = \frac{\rho_{p,h}}{f_{scale} \cdot \rho_{p,c}} \Delta p_{g,c}, \tag{4.4}$$

where "h" and "c" stands for the hot and cold pressure drops and densities in the 100 kW unit and cold-flow model, respectively. Here, $f_{scale} = \Delta h_c / \Delta h_h$ is the scale factor 0.577. The densities used were $\rho_{p,c} = 2.65$ g/cm^3 and $\rho_{p,h} = 3.60$ g/cm^3, as the ilmenite in the 100 kW unit is assumed to have not been fully activated.

In order to compare pressure drops between the cold-flow model and the 100 kW unit, dynamic similarity must exist between the units. The pressure profile in Paper II comes from experiments using air as fluidisation gas. For this study, it is hence assumed that the requirement to use helium can be relaxed for the purpose of comparing pressure drops. Fig. 4.9(a) shows the pressure profile from Paper II, scaled up using Eq. (4.4), and Fig. 4.9(b) shows a pressure profile created from the first operational period with the Colombian coal in Paper III. Both profiles are adapted so that 0 kPa gauge pressure is defined for the top of the fuel reactor cyclone. The numbers in the profiles match the

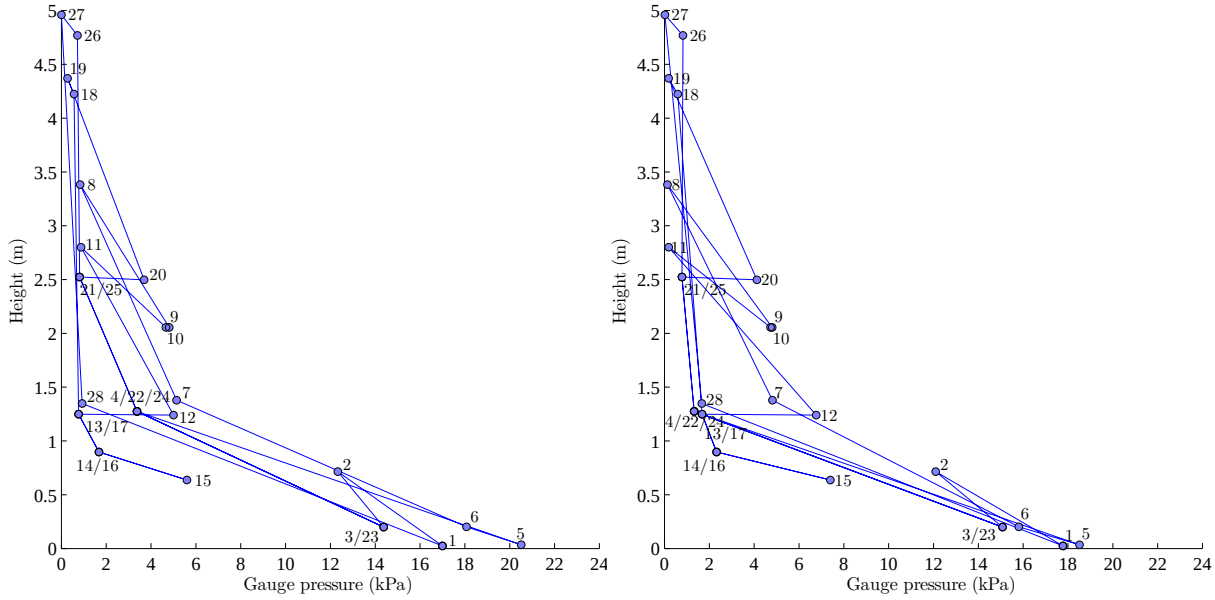

(a) (b)

Fig. 4.9: (a) Upscaled pressure profiles from a cold-flow model experiment, adapted from Paper II and (b) the first operational period with Colombian coal in the 100 kW unit.

numbers provided in Fig. 2.2. From a comparison between the profiles in Fig. 4.9(a) and Fig. 4.9(b), it is clear that the cold-flow model gives a good representation of the pressure profile in the 100 kW unit.

4.7 Relation between circulation, bed height and gas conversion (Paper VI)

As previously mentioned, the 100 kW unit has significant flexibility with respect to a number of operational parameters in operation. Due to this flexibility, Section 4.4 could conclude that the gas conversion is strongly dependent on the bed inventory in the fuel reactor. Three fluidisation flows of major importance for the system behaviour are identified. They are the flows in the air reactor, the fuel reactor and the circulation riser. To present their interrelation more clearly, effects from changing key operational parameters are presented here, focusing on gas conversion, fuel reactor bed inventory and global solids circulation. Here, gas conversion is represented by the oxygen demand ($\gamma = 1 - \Omega_{OD}$), the fuel reactor bed inventory is represented by the total pressure drop, Δp, while the circulation, $\dot{m}$, was calculated from the air reactor riser pressure drop, see Eq. (4.3).

4.7.1 Varying the air reactor flow

Fig. 4.10 shows the response in oxygen demand, fuel reactor pressure drop and circulation when doing step-wise changes in the air reactor fluidisation flow as seen in several operational periods (Paper V). Using data from the Cerrejón operational periods VI, VII and IX, three set of lines are presented. Each set is taken from a different operational period. The air reactor fluidisation flow was varied and everything else was kept constant. The flow was changed from 1660 L_n/min to 2500 L_n/min. As can be seen, each increase in the air reactor flow results in a higher circulation, which leads to a larger bed inventory in the fuel reactor, which in turn leads to a lower oxygen demand.

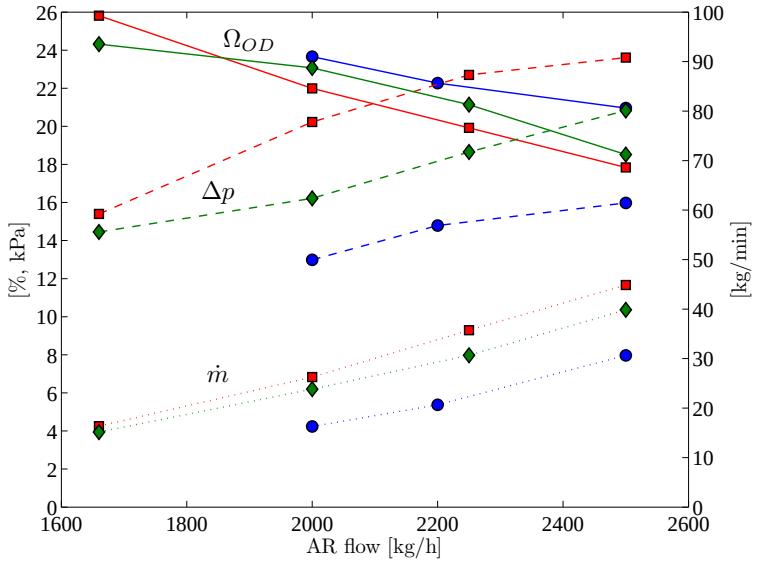

Fig. 4.10: Responses in the oxygen demand (solid lines), fuel reactor pressure drop (dashed lines) and circulation (dotted lines) when varying the air reactor fluidisation flow. Data from periods VI (blue circles), VII (red squares) and IX (green diamonds).

4.7.2 Varying the fuel reactor flow

In a similar manner as for the air reactor fluidisation flow, Fig. 4.11 shows the response in oxygen demand, fuel reactor pressure drop and circulation when doing a step-wise change in the fuel reactor fluidisation flow as seen in several operational periods. The flow was changed in a range between 5 kg/h to 20 kg/h. As can be seen, an increase in the fuel reactor flow does not seem to have a large effect on the investigated variables. However, a slight increase in oxygen demand is observable. To summarise, the results all show that the effect of changing the fuel reactor flow is small.

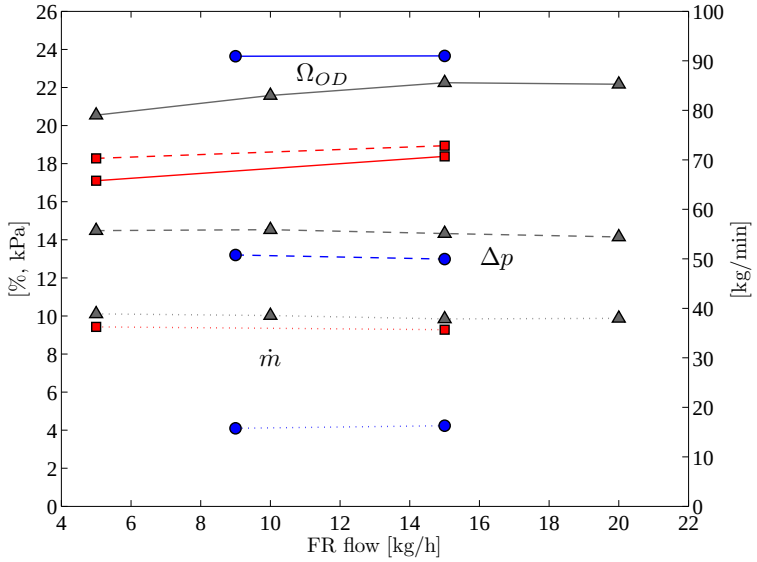

Fig. 4.11: Responses in the oxygen demand (solid lines), fuel reactor pressure drop (dashed lines) and circulation (dotted lines) when varying the fuel reactor fluidisation flow. Data from periods VI (blue circles), VII (red squares) and X (grey triangles).

4.7.3 Varying the circulation riser flow

Fig. 4.12 shows the response in oxygen demand, fuel reactor pressure drop and circulation when doing step-wise changes in the circulation riser fluidisation flow as seen in several operational periods. The flow was changed in a range between 3 kg/h to 10 kg/h. As can be seen, each increase in the circulation riser flow results in a higher circulation. However, contrary to the events seen in Fig. 4.10 when changing the air reactor fluidisation flow, the increased circulation leads to a lower fuel reactor bed inventory, which in turn leads to a higher oxygen demand. This shows that a low oxygen demand, i.e. a high gas conversion, can be achieved even with a low overall circulation, provided that the circulation riser flow is adjusted to impose a large bed inventory in the fuel reactor.

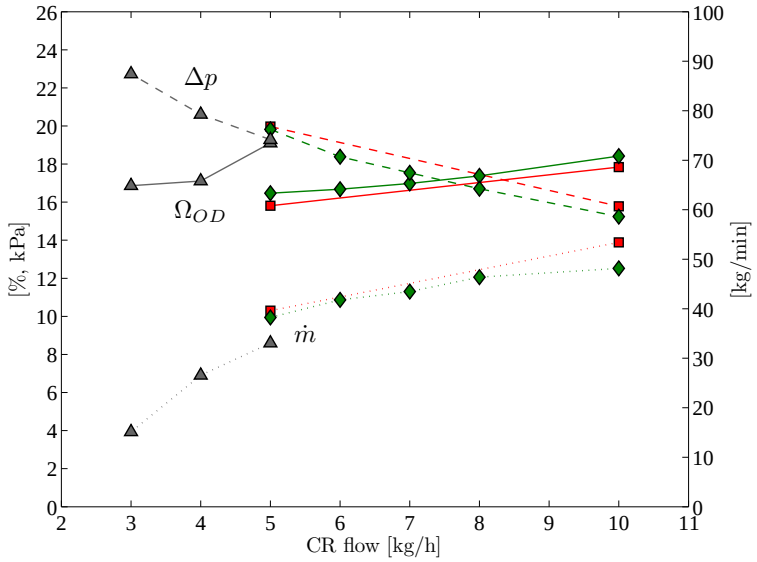

Fig. 4.12: Responses in the oxygen demand (solid lines), fuel reactor pressure drop (dashed lines) and circulation (dotted lines) when varying the circulation riser fluidisation flow. Data from periods VII (red squares), IX (green diamonds) and X (grey triangles).

4.7.4 Evaluating the gas conversion model

In Section 3.3, a model for gas conversion was discussed. To test the model, both for char as well as for char and volatiles together, data are collected from the operational periods analysed in Papers IV–V. Through α and κ, the model contains a dependence on the fluidisation flow of steam, F_0. This flow is assumed to pass evenly through the bed. In real fluidisation, steam with a superficial velocity in excess of u_{mf} will form bubbles and will not have an ideal contact with the bed material. Furthermore, as discussed in Section 4.7.2, the oxygen demand does not seem to depend on the FR flow. For this study, the base case $F_0 = 5$ kg/h was used in the model. Other constants used in the model are given in Table 4.3. Here, the values for k_F are taken or calculated from [77, 78]. The model

Table 4.3: Summary of the model parameters used. Here, k_F is given in $\mathrm{m_n^3/(tonne{\cdot}s)}$.

Parameter	Char model	Full model	
	γ_c	γ_c	γ_v
$k_{F,CO}$	3	3	3
k_{F,H_2}	15	15	15
k_{F,CH_4}	-	-	0.3
κ	0.066	1.35	1.35
$\phi_{s,core}$	0.16	0.16	0.15
ξ	-	0.85	

results, using Eq. (3.25) and Eq. (3.28), are presented in Fig. 4.13. Using the Cerrejón periods, data from eight of the ten available γ's of pure char conversion as well as data

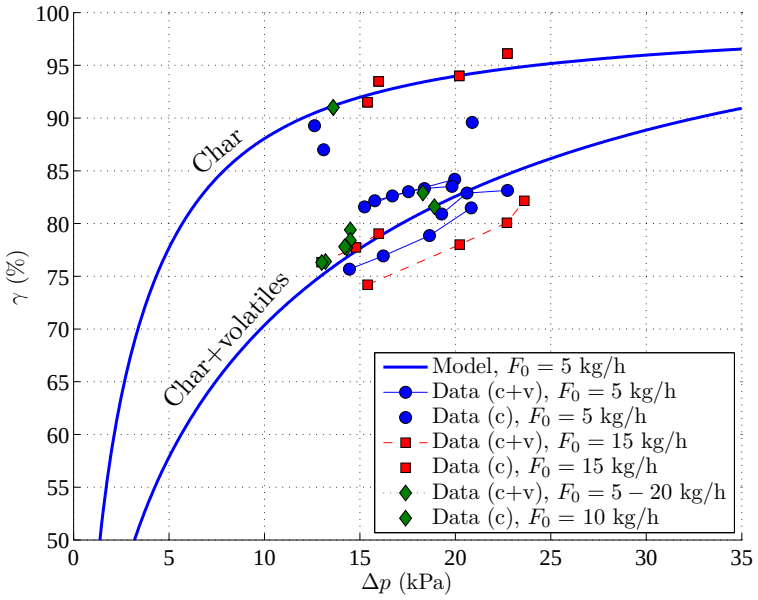

Fig. 4.13: All available data from full fuel and pure char conversion together with the corresponding models.

from Figs. 4.10–4.12 are appended for comparison. Fig. 4.13 shows that the model fits the experiments well. The full model suggests that a 90% gas conversion would be reached at 32–33 kPa pressure drop in the fuel reactor.

5

Discussion and conclusions

5.1 Discussion

5.1.1 Motivation of work

This thesis describes the design, modelling and operation of a 100 kW chemical-looping combustor for solid fuels. The thesis begins by discussing the concerns of global warming and its relation to the increasing rate of greenhouse gas release to the atmosphere. Among the greenhouse gases being released, CO_2 is the most important one. Point-source CO_2 is released mainly through the use of fossil fuels in energy production and through heavy industrial processes, such as cement and steel production. Chemical-looping combustion is a CO_2 capture technology that can be used in e.g. large scale power plants using a technology with clear similarities to circulating fluidised bed (CFB) boilers. CFB boilers have a size of up to 460 MW_{el} [79], although larger sizes would be feasible. The great advantage of chemical-looping combustion, compared to other capture technologies, lies in the fact that no active gas separation is needed, thus avoiding both high costs and energy penalties.

5.1.2 Concerning flexibility and stability of operation

The 100 kW unit is a pilot-scale test rig, designed for flexibility in operation. The advantages of having operational flexibility are many. There are several variables that are known to affect gas conversion and CO_2 capture efficiency in a chemical-looping combustor. Perhaps the most important ones are fuel reactor temperature, global solids circulation and fuel reactor bed inventory. These three variables are intrinsically interlinked and experiments were necessary to clarify their interrelation. However, from a design point of view, the engine for global circulation is the air reactor. From here, freshly oxidised particles are transported to the fuel reactor. Global solids circulation is important for the heat balance between the air and fuel reactors. As heat is produced in the air reactor and normally consumed in the fuel reactor, it is important to have sufficient circulation in order to avoid a decrease in the fuel reactor temperature, leading to adverse effects on performance.

Through experiments in the cold-flow model, it was learnt that the solids inventories in the fuel and air reactors of the cold-flow model are stable to changes in the fluidisation velocity, i.e. the system is self-stabilising in a large range of circulation mass flows. This

means that for each flow change, a new steady-state is automatically assumed. Thus, there seems to be little risk of emptying any of the reactors. However, it is still possible to vary the bed inventories, i.e. to transfer bed material between the fuel and air reactors in a certain span. The key to regulate this transfer lies in the circulation riser fluidisation flow, as it constitutes a bottleneck for the global solids circulation and may be used to control the bed inventory in the fuel reactor.

5.1.3 Comments on the loss of unconverted gases

Analyses of the experiments, conducted in the 100 kW unit so far, have shown a significant concentration of unconverted gases exiting the fuel reactor. The presence of these unconverted gases are expected and can be remediated in the following ways:

- By oxygen polishing, i.e. addition of oxygen at the outlet of the fuel reactor.
- By separation and recycling of unconverted gas in connection to CO_2 compression.
- By the use of an oxygen carrier that releases oxygen (CLOU).
- By leading the gas from the fuel reactor to an additional fuel reactor, lying in series with the first one.

It should be noted that there are also a number of ways to modify the design and operation of the fuel reactor, including the use of, or mixing with, other oxygen carriers that could improve gas conversion [9, 33].

5.2 Conclusions

In Paper I–VI, many aspects of chemical-looping combustion for solid fuels are investigated. Three units were available for the research. One smaller 10 kW unit, one cold-flow model to study system behaviour under variations of operational parameters, and finally a 100 kW pilot-scale test rig. Below is a summary of the most important findings that are directly related to the study of the 100 kW unit.

An application of a multistage-bed model for a residence-time analysis in chemical-looping combustion was developed. Fuel was added batch-wise to the 10 kW unit, where gas concentrations exiting the air reactor were analysed. Conclusions include that

- It was possible to determine the residence-time and residence-time distribution of particles in the fuel reactor for a number of operational cases with different solids circulation.
- Knowing the solids inventory in the fuel reactor, the circulation mass flow could also be determined.
- The circulation mass flow could be directly correlated to the riser mass flow, determined from pressure drop measurements in the riser.

The method used to derive a correlation between the mass flow calculated from batch experiments and the mass flow calculated from air reactor pressure drops proved useful as it enables the mass flow to be calculated in real-time during operation. The mass flow can then be correlated to other parameters such as temperature or gas conversion.

The cold-flow model was built specifically to prepare for the operation of the 100 kW unit. The cold-flow model residence-time in the fuel and air reactor sections were found to be variable in a wide range, between 2–11 minutes and 3–21 minutes, respectively, for the investigated fluidisation velocities of the air reactor. Both these results indicated that operation in the 100 kW unit would show similar behaviour. Finding that the circulation mass flows were approximately linear in the riser mass flow, as determined by pressure drops, was an important result. It strengthened the validity to use the correlation between mass flow, calculated from a batch experiment, and mass flow calculated from pressure drops.

In the 100 kW unit, three operational periods were conducted with one bituminous coal from Colombia, one period with a petroleum coke from Mexico and ten periods with another bituminous coal from Colombia, labelled "Cerrejón coal". The last one was the design coal for the 100 kW unit and represented over 85% of the total operational time, conducted within the scope of this thesis. The experiments with the first Colombian coal were focused on testing the stability of the unit. At this point, no attempts were made to use the flexibility of the system to optimise performance. As seen in Table 4.2, typical operational conditions were fuel reactor pressure drops and temperatures varying between 12–15 kPa and 930–950℃, with a global solids circulation varying between 7–16 kg/min. From the experiments conducted, it was found that

- Operation was stable and continuous fuel feeding for over 1 h was possible.
- A gas conversion and CO_2 capture efficiency of up to 81.5% and 96.0%, respectively, were found from averaging the performance indicators during the final minutes of operation.

The incomplete gas conversion means that there is a loss of unconverted CO, H_2 and CH_4 from the fuel reactor. Using ilmenite as oxygen carrier, the concentration of CO is expected to be higher than that of H_2. However, the high concentration of H_2O from the fluidisation gas likely raises the H_2 concentration through the water-gas shift reaction. A significant part of the unconverted gas comes from the volatiles, as seen from the sharp decrease in oxygen demand when the fuel feed is stopped.

As mentioned above, only one experiment with a Mexican petroleum coke was conducted. The purpose was to test a very different fuel before moving on with the design fuel, the Cerrejón coal. The petroleum coke has a high char content and thus a low volatiles content. In addition, it is rich in sulphur and low on ash. Experience from such a fuel is useful when discussing performance results and connecting them with the fuel composition. Conclusions include:

- The Mexican petroleum coke, which has a lower volatiles content, showed a clearly lower oxygen demand compared to the Colombian coal. This agrees also with the first observations that the oxygen demand falls to around 10% after fuel stop, i.e. when the volatiles disappear.
- An average gas conversion and CO_2 capture efficiency of 85.2% and 77.7%, respectively, were found at a fuel reactor pressure drop and temperature of around 11 kPa and 926℃, with a global solids circulation of 10–11 kg/min.
- No adverse effects of reaching an air reactor temperature of 1050°C were detected.

From the ten operational periods with the bituminous Cerrejón coal, most conclusions could be drawn from the final five periods. These periods were significantly longer than the first five due to the implementation of a larger fuel container. As seen in Table 4.2, typical operational conditions in the final five periods were fuel reactor pressure drops and temperatures varying between between 15–23 kPa and 944–964℃, with a global solids circulation varying between 16–40 kg/min. Important conclusions include:

- A gas conversion and CO_2 capture efficiency of over 84% and 99%, respectively, were found from averaging the performance indicators during the final minutes of operation.
- Tests replacing all nitrogen sources with CO_2 showed that the sum of measured gases was very close to 100%, indicating that only minute quantities of other species were released.
- Results of the effect of steam gasification in the carbon stripper showed a clear improvement in the CO_2 capture efficiency, indicating an increase from 95.5% to 98.5%. This test involved switching the fluidisation flow from steam to nitrogen, thus the char separation of the carbon stripper was assumed to be similar.
- The system allows for an independent control of global solids circulation and solids inventory in the fuel reactor by using the flows fluidising the AR and CR.
- It is shown that increased air reactor flow increases the global solid circulation. This leads to a transfer of bed material from the air reactor to the fuel reactor, provided that the circulation riser flow is constant.
- Increasing the fuel reactor flow leads to a moderate decrease in gas conversion but the CO_2 capture seems largely unaffected.
- By raising the circulation riser flow, global solids circulation is drastically increased.
- A careful analysis was made on the relation between fluidisation flows, global solids circulation, fuel reactor bed inventory and gas conversion. The results show that it is the bed inventory in the fuel reactor, rather than the global solids circulation, which has the major impact on gas conversion.
- Despite several minutes without fluidisation in the many sections of the reactor system fluidised by steam, operation could be resumed without any indications of harm having come to the oxygen carrier.
- With measured concentrations of NO, typically in the range of 1000–2000 ppm, it can be concluded that roughly 10–20% of the fuel-N is oxidised to NO for the Cerrejón coal.

Nomenclature

A_c	Cross-section area (m^2)
BET	Specific surface area (m^2/g)
C_k	Concentration of particles after the k:th CSTR (mol/m^3)
CI	Circulation index (kPa·L/min)
$\bar{d}_p$	Average particle diameter (μm)
D	Bed diameter (m)
Fr	The Froude number, $u_0/\sqrt{gD}$ (-)
F_0, $\dot{V}_0$	Fluidisation flow of steam (kg/h or L_n/min)
F_g, $\dot{V}_g$	Total flow of gas, originating from the gasification or devolatilisation of the fuel (L_n/min)
F_j	Volumetric flow of gas in reactor j (L_n/min)
$F_{AR,out}$	Volumetric flow of gas in the air reactor (L/min)
f_{scale}	The scale factor determined by the full set of scaling laws (-)
g	Gravitational acceleration (m/s^2)
G_s	Particle mass flux ($kg/(m^2 \cdot s)$)
Δh	Distance between two pressure taps in the riser (m)
$k_{F,i}$	Mass-based reaction rate constant between the ilmenite oxygen carrier and an unconverted species i (m_n^3/(tonne·s))
L	Characteristic bed length, e.g. height (m)
LHV	Lower heating value (MJ/kg)
$\dot{m}$, $\dot{m}_{AR}$	Global solids circulation (kg/min)
$\dot{m}_{FR}$	Circulation mass flow in the FR loop (kg/min)
$\dot{m}_{G_s}$, $\dot{m}_{riser}$	(Estimated) riser mass flow, i.e. mass flow based on the pressure drop in a riser (kg/min)
m	Mass (kg)
$m_{0,ox}/m_{0,red}$	Mass of a fully oxidised/reduced oxygen carrier particle (kg)

m_τ	Total bed mass from the point of fuel insertion till the entry of the air reactor (kg)
$\dot{n}_k$	Molar flow of particles after the k:th CSTR (mol/s)
N	Fitting parameter in the residence-time analysis (-)
Δp_g	Gauge pressure/pressure difference to a reference pressure (kPa)
$\Delta P_{\Delta h}$, Δp_{riser}	Riser pressure drop over Δh (kPa)
p_i	Partial pressure of species i (Pa)
$p_{i,max}$	Maximum partial pressure of species i (Pa)
Q	Overall volume flow (m^3/s)
Re_D	Reynolds number based on bed diameter, $\rho_f u_0 D/\mu_f$ (-)
Re_{d_p}	Reynolds number based on particle diameter, $\rho_p u_0 d_p/\mu_f$ (-)
R_0	Oxygen transfer capacity of the oxygen carrier (%)
u_0	Superficial gas velocity (m/s)
u_t	Terminal velocity of the oxygen carrier particles (m/s)
u_{mf}	Minimum fluidisation velocity (m/s)
V_k	Volume of the k:th CSTR (m^3)
$x_{i,j}$	Molar fraction of species i in reactor j (-)

Greek letters

α_i	Dimensionless number, indicating the potential for an unconverted gas i to convert (-)
γ	Gas conversion for the fuel (%)
γ_c	Gas conversion for char syngas (%)
γ_v	Gas conversion for volatiles (%)
γ_ϕ	Gas conversion for the fuel, corrected for gas bypass and char loss (%)
$\gamma_{c,i}$	Gas conversion for species i in char syngas (%)
$\gamma_{v,i}$	Gas conversion for species i in volatiles (%)
ϵ	Bed voidage (-)
ϵ_{eff}	Effective voidage between fluidised particles up to the reference pressure (-)
η_{CC}	Carbon capture efficiency (%)
η_{OO}	Oxide oxygen/CO_2 capture efficiency (%)

κ	Volumetric fraction of gas, produced by the fuel, to the fluidisation flow of steam (-)
μ_f	Dynamic viscosity of the fluidisation gas (μPas)
ξ	Fraction of char converted, i.e. not lost to the filters (-)
ρ_b	Bulk density (kg/m^3)
ρ_f	Fluidisation gas density (kg/m^3)
ρ_p	(Effective) particle density (kg/m^3)
ρ_t	True density (kg/m^3)
τ	Residence time between the point of fuel insertion till the entry of the air reactor (min)
τ_k	Residence-time in the k:th CSTR (min)
ϕ	Particle sphericity (-)
$\phi_{s,core}$	Fraction of solids exposed to the gas passing in plug flow (-)
φ	Particle porosity (-)
Φ_0	Oxygen/carbon ratio, i.e. the ratio of moles of oxygen needed to convert the fuel completely per moles of carbon in the fuel (-)
Ω_{OD}	Oxygen demand (1 − gas conversion) (%)

Abbreviations

AR	Air reactor
C-gas	The sum of CO_2, CO and CH_4
CCS	Carbon capture and storage
CDCL	Coal direct chemical-looping
Ce	Cerrejón coal
CFB	Circulating fluidised bed
CFM	Cold-flow model
CLC	Chemical-looping combustion
CLOU	Chemical-looping with oxygen uncoupling
Co	Colombian coal
CR	Circulation riser
CS	Carbon stripper
CSTR	Continuous stirred-tank reactor

CY	Cyclone
FR	Fuel reactor
HIVEL	High velocity
LOVEL	Low velocity
LS	Loop seal
M	Mexican petroleum coke
PFR	Plug flow reactor
PSD	Particle size distribution
SEM	Scanning electron microscope

Bibliography

[1] K. E. Trenberth, P. D. Jones, P. Ambenje, R. Bojariu, D. Easterling, A. Klein Tank, D. Parker, F. Rahimzadeh, J. A. Renwick, M. Rusticucci, B. Soden, and P. Zhai. Contribution of working group I to the fourth assessment report of the intergovernmental panel on climate change. In S. Solomon, D. Qin, M. Manning, Z. Chen, M. Marquis, K. B. Averyt, M. Tignor, and H. L. Miller, editors, *Climate Change 2007: The Physical Science Basis*, chapter Observations: Surface and Atmospheric Climate Change. Cambridge University Press, Cambridge, United Kingdom and New York, NY, USA, 2007.

[2] H. Le Treut, R. Somerville, U. Cubasch, Y. Ding, C. Mauritzen, A. Mokssit, T. Peterson, and M. Prather. Contribution of working group I to the fourth assessment report of the intergovernmental panel on climate change. In S. Solomon, D. Qin, M. Manning, Z. Chen, M. Marquis, K. B. Averyt, M. Tignor, and H. L. Miller, editors, *Climate Change 2007: The Physical Science Basis*, chapter Historical Overview of Climate Change Science. Cambridge University Press, Cambridge, United Kingdom and New York, NY, USA, 2007.

[3] P. Forster, V. Ramaswamy, P. Artaxo, T. Berntsen, R. Betts, D. W. Fahey, J. Haywood, J. Lean, D. C. Lowe, G. Myhre, J. Nganga, R. Prinn, G. Raga, M. Schulz, and R. Van Dorland. Contribution of working group I to the fourth assessment report of the intergovernmental panel on climate change. In S. Solomon, D. Qin, M. Manning, Z. Chen, M. Marquis, K. B. Averyt, M. Tignor, and H. L. Miller, editors, *Climate Change 2007: The Physical Science Basis*, chapter Changes in Atmospheric Constituents and in Radiative Forcing. Cambridge University Press, Cambridge, United Kingdom and New York, NY, USA, 2007.

[4] United Nations Framework Convention on Climate Change. Copenhagen accord. Technical report, Decision 2/CP.15, 2009.

[5] B. Metz, O. Davidson, H. C. de Coninck, M. Loos, and L. A. Meyer, editors. *IPCC Special Report on Carbon Dioxide Capture and Storage*. Cambridge University Press, Cambridge, United Kingdom and New York, NY, USA, 2005. Prepared by Working Group III of the Intergovernmental Panel on Climate Change.

[6] F. Kozak, A. Petig, E. Morris, R. Rhudy, and D. Thimsen. Chilled ammonia process for CO2 capture. *Energy Procedia*, 1(1):1419–1426, 2009.

[7] Q. Zafar, T. Mattisson, and B. Gevert. Integrated hydrogen and power production with CO2 capture using chemical-looping reforming - Redox reactivity of particles of

CuO, Mn2O3, NiO, and Fe2O3 using SiO2 as a support. *Ind. Eng. Chem. Res.*, 44 (10):3485–3496, 2005.

[8] M. Rydén and A. Lyngfelt. Using steam reforming to produce hydrogen with carbon dioxide capture by chemical-looping combustion. *International Journal of Hydrogen Energy*, 31(10):1271–1283, 2006.

[9] C. Linderholm, A. Lyngfelt, A. Cuadrat, and E. Jerndal. Chemical-looping combustion - operation in 10 kW unit with two fuels, above-bed and in-bed fuel feed and two oxygen carriers, manganese ore and ilmenite. *Fuel*, 102:808–822, 2012.

[10] N. Berguerand and A. Lyngfelt. Batch testing of solid fuels with ilmenite in a 10 kWth chemical-looping combustor. *Fuel*, 89(8):1749–1762, 2010.

[11] P. Moldenhauer, M. Rydén, T. Mattisson, and A. Lyngfelt. Chemical-looping combustion and chemical-looping reforming of kerosene in a circulating fluidized-bed 300 W laboratory reactor. *International Journal of Greenhouse Gas Control*, 9:1–9, 2012.

[12] W. K. Lewis and E. R. Gilliland. Production of pure carbon dioxide. US Patent: 2 665 971, 1954. S.O.D Company.

[13] M. Ishida, D. Zheng, and T. Akehata. Evaluation of a chemical-looping combustion power-generation system by graphic energy analysis. *Energy*, 12(2):147–154, 1987.

[14] M. Ishida and H. Jin. A novel combustor based on chemical-looping combustion reactions and its reactions kinetics. *Journal of Chemical Engineering of Japan*, 27 (3):296–301, 1994.

[15] A. Lyngfelt, B. Leckner, and T. Mattisson. A fluidized-bed combustion process with inherent CO2 separation; application of chemical-looping combustion. *Chem. Eng. Sci*, 56:3101–3113, 2001.

[16] A. Lyngfelt and T. Mattisson. Materials for chemical-looping combustion. In D. Stolten and V. Scherer, editors, *Process Engineering for CCS Power Plants*, pages 475–504. WILEY-VCH Verlag GmbH & Co. KGaA, 2011.

[17] A. Lyngfelt. Oxygen carriers for chemical looping combustion - 4 000 h of operational experience. *Oil & Gas Science and Technology - Rev. IFP Energies nouvelles*, 66(2): 161–172, 2011.

[18] A. Hoteit, A. Forret, W. Pelletant, J. Roesler, and T. Gauthier. Chemical-looping combustion with different types of liquid fuels. *Oil & Gas Science and Technology - Rev. IFP Energies nouvelles*, 66(2):193–199, 2011.

[19] P. Moldenhauer, M. Rydén, T. Mattisson, and A. Lyngfelt. Chemical-looping combustion and chemical-looping with oxygen uncoupling of kerosene with Mn- and Cu-based oxygen carriers in a circulating fluidized-bed 300 W laboratory reactor. *Fuel Processing Technology*, 104:378–389, 2012.

[20] H. Leion, T. Mattisson, and A. Lyngfelt. The use of petroleum coke as fuel in chemical-looping combustion. *Fuel*, 86:1947–1958, 2007.

[21] Y. Cao, Z. Chen, J. T. Riley, and W. P. Pan. Reduction of solid oxygen carrier (CuO) by solid fuel (coal) in chemical-looping combustion. *Preprints of Symposia - American Chemical Society*, 50(1):99–102, 2005.

[22] R. K. Lyon and J. A. Cole. Unmixed combustion: an alternative to fire. *Combustion and Flame*, 121:249–261, 2000.

[23] Y. Cao, K. L. Liu, J. T. Riley, and W. P. Pan. Application of a circulating fluidized-bed process for the chemical-looping combustion of solid fuels. *Preprints of Symposia - American Chemical Society*, 49(2):815–816, 2004.

[24] J. M. Mou, W. G. Xiang, and T. T. Di. Performance study of an oxygen-bearing iron oxide-based combined cycle system featuring integrated coal-gasification chemical-looping combustion. *Journal of Engineering for Thermal Energy & Power*, 22(2): 149–153, 2007.

[25] J. S. Dennis, S. A. Scott, and A. N. Hayhurst. In situ gasification of coal using steam with chemical-looping: a technique for isolating CO2 from burning a solid fuel. *J. Energy Inst.*, 79(3):187–190, 2006.

[26] S. A. Scott, J. S. Dennis, and A. N. Hayhurst. In situ gasification of solid fuel and CO2 separation using chemical-looping. *AIChE Journal*, 52(9):3325–3328, 2006.

[27] Z. P. Gao, L. H. Shen, J. Xiao, C. J. Qing, and Q. L. Song. Use of coal as fuel for chemical-looping combustion with Ni-based oxygen carrier. *Industrial and Engineering Chemistry Research*, 47(23):9279–9287, 2008.

[28] J. Wu, L. Shen, J. Hao, and H. Gu. Chemical looping combustion of coal in a 1 kWth reactor. In *1st International Conference on Chemical Looping*, Lyon, France, 17–19 March 2010.

[29] H. Gu, L. Shen, J. Xiao, S. Zhang, and T. Song. Chemical looping combustion of biomass/coal with natural iron ore as oxygen carrier in a continuous reactor. *Energy Fuels*, 25(1):446–455, 2011.

[30] A. Cuadrat, A. Abad, F. García-Labiano, P. Gayán, L. F. de Diego, and J. Adánez. The use of ilmenite as oxygen-carrier in a 500 Wth chemical-looping coal combustion unit. *International Journal of Greenhouse Gas Control*, 5(6):1630–1642, 2011.

[31] A. Abad, I. Adánez-Rubio, P. Gayán, F. García-Labiano, L. F. de Diego, and J. Adánez. Demonstration of chemical-looping with oxygen uncoupling (CLOU) process in a 1.5 kW th continuously operating unit using a Cu-based oxygen-carrier. *International Journal of Greenhouse Gas Control*, 6:189–200, 2012.

[32] N. Berguerand and A. Lyngfelt. Design and operation of a 10 kWth chemical-looping combustor for solid fuels - Testing with South African coal. *Fuel*, 87(12):2713–2726, 2008.

[33] A. Cuadrat, C. Linderholm, A. Abad, A. Lyngfelt, and J. Adánez. Influence of limestone addition in a 10 kwth chemical-looping combustion unit operated with petcoke. *Energy Fuels*, 25(10):4818–4828, 2011.

[34] L. H. Shen, J. H. Wu, and J. Xiao. Experiments on chemical looping combustion of coal with a NiO based oxygen carrier. *Combustion and Flame*, 156(3):721–728, 2009.

[35] J. Wu, L. Shen, J. Xiao, L. Wang, and J. Hao. Chemical looping combustion of sawdust in a 10 kWth interconnected fluidized bed. *Huagong Xuebao/CIESC Journal*, 60(8):2080–2088, 2009.

[36] T. Sozinho, W. Pelletant, H. Stainton, F. Guillou, and T. Gauthier. Main results of the 10 kWth coal pilot plant operation. In *2nd International Conference on Chemical Looping*, Darmstadt, Germany, 26–28 September 2012.

[37] A. Thon, M. Kramp, E.-U. Hartge, S. Heinrich, and J. Werther. Operational experience with a coupled fluidized bed system for chemical looping combustion of solid fuels. In *2nd International Conference on Chemical Looping*, Darmstadt, Germany, 26–28 September 2012.

[38] A. Tong, S. Bayham, M. V. Kathe, S. W. Luo L. Zeng, and L.-S. Fan. Iron-based syngas chemical looping process and coal-direct chemical looping process development at Ohio State University. In *2nd International Conference on Chemical Looping*, Darmstadt, Germany, 26–28 September 2012.

[39] L. Zeng, M. V. Kathe, E. Y. Chung, and L.-S. Fan. Some remarks on direct solid fuel combustion using chemical looping processes. *Current Opinion in Chemical Engineering*, 1(3):290–295, 2012.

[40] J. Adánez, A. Abad, F. Garcia-Labiano, P. Gayan, and L. de Diego. Progress in chemical-looping combustion and reforming technologies. *Progress in Energy and Combustion Science*, 38(2):215–282, 2012.

[41] A. Lyngfelt. Chemical looping combustion. In F. Scala, editor, *Fluidized-bed technologies for near-zero emission combustion and gasification*, chapter 20. Woodhead Publishing, 2012. Submitted for inclusion.

[42] L.-S. Fan, L. Zeng, W. Wang, and S. W. Luo. Chemical looping processes for CO2 capture and carbonaceous fuel conversion - prospect and opportunity. *Energy & Environmental Science*, 5:7254–7280, 2012.

[43] M. Orth, J. Ströhle, and B. Epple. Design and operation of a 1 MWth chemical looping plant. In *2nd International Conference on Chemical Looping*, Darmstadt, Germany, 26–28 September 2012.

[44] H. Andrus, J. Chui, P. Thibeault, C. Edberg, D. Turek, J. Kenney, I. Abdulally, P. Chapman, S. Kang, and B. Lani. Alstom's limestone-based chemical looping process. In *2nd International Conference on Chemical Looping*, Darmstadt, Germany, 26–28 September 2012.

[45] CCEMC announces $46 million in funding for carbon capture and storage and cleaner energy projects. Available from the Internet: http://ccemc.ca, 12 July 2012. Accessed 16 October 2012.

[46] S. P. Sit, A. Reed, U. Hohenwarter, V. Horn, K. Marx, and T. Pröll. 10 MW CLC field pilot. In *2nd International Conference on Chemical Looping*, Darmstadt, Germany, 26–28 September 2012.

[47] J.-X. Morin, C. Beal, and S. Suraniti. 455 MWe CLC boiler / plant feasibility report and recommendations for the next step. Technical report, ENCAP deliverable D4.2.4, Available from Internet: http://www.encapco2.org, 2005. Accessed 15 October 2012.

[48] E. Buckingham. On physically similar systems; illustrations of the use of dimensional analysis. *Phys. Rev.*, 4:345–376, 1914.

[49] L. R. Glicksman. Scaling relationships for fluidized beds. *Chemical Engineering Science*, 39(9):1373–1379, 1984.

[50] R. Jackson. Fluid mechanical theory. In J. F. Davidson and D. Harrison, editors, *Fluidization*. Academic Press, New York, 1971.

[51] M. Horio, A. Nonaka, Y. Sawa, and I. Muchi. New similarity rule for fluidized bed scale-up. *AIChE Journal*, 32(9):1466–1482, 1986.

[52] L. R. Glicksman. Scaling relationships for fluidized beds. *Chemical Engineering Science*, 43(6):1419–1421, 1988.

[53] M. Horio, H. Ishii, Y. Kobukai, and N. Yamanishi. A scaling law for circulating fluidized beds. *Journal of Chemical Engineering of Japan*, 22(6):587–592, 1989.

[54] L. R. Glicksman, M. Hyre, and K. Woloshun. Simplified scaling relationships for fluidized beds. *Powder Technology*, 77:177–199, 1993.

[55] L. R. Glicksman, M. R. Hyre, and P. A. Farrell. Dynamic similarity in fluidization. *International Journal of Multiphase Flow*, 20:331–386, 1994.

[56] T. J. Fitzgerald, D. Bushnell, S. Crane, and Y.-C. Shieh. Testing of cold scaled bed modeling for fluidized-bed combustors. *Powder Technology*, 38(2):107–120, 1984.

[57] F. Johnsson, A. Vrager, and B. Leckner. Solids flow pattern in the exit region of a CFB-furnace - influence of exit geometry. In *16th International Conference on Fluidized Bed Combustion*, Savannah, USA, 16–19 May 1999.

[58] B. Leckner, P. Szentannai, and F. Winter. Scale-up of fluidised-bed combustion - a review. *Fuel*, 90:2951–2964, 2011.

[59] T. Pröll, K. Rupanovits, P. Kolbitsch, J. Bolhàr-Nordenkampf, and H. Hofbauer. Cold flow model study on a dual circulating fluidized bed system for chemical looping process. *Chemical Engineering & Technology*, 32(3):418–424, 2009.

[60] E. Jerndal, T. Mattisson, and A. Lyngfelt. Thermal analysis of chemical-lopping combustion. *Chemical Engineering Research and Design*, 84(9):795–806, 2006.

[61] T. Mattisson, M. Johansson, and A. Lyngfelt. CO2 capture from coal combustion using chemical-looping combustion - reactivity investigation of Fe, Ni and Mn based oxygen carriers using syngas. In *Clearwater Coal conference*, Clearwater, USA, 2006.

[62] H. Leion, A. Lyngfelt, and T. Mattisson. Solid fuels in chemical-looping combustion using a NiO-based oxygen carrier. *Chemical Engineering Research and Design*, 87: 1543–1550, 2009.

[63] T. Mattisson, A. Lyngfelt, and H. Leion. Chemical-looping with oxygen uncoupling for combustion of solid fuels. *International Journal of Greenhouse Gas Control*, 3(1): 11–19, 2009.

[64] M. Rydén, A. Lyngfelt, and T. Mattisson. $CaMn_{0.875}Ti_{0.125}O_3$ as oxygen carrier for chemical-looping combustion with oxygen uncoupling (CLOU) - experiments in a continuously operating fluidized-bed reactor system. *International Journal of Greenhouse Gas Control*, 5(2):356–366, 2011.

[65] G. Azimi, H. Leion, T. Mattisson, and A. Lyngfelt. $(Mn_yFe_{1-y})O_x$ combined oxides as oxygen carrier for chemical-looping combustion with oxygen uncoupling (CLOU). *Accepted for publication in AIChE Journal*, 2012.

[66] C. Linderholm, T. Mattisson, and A. Lyngfelt. Long-term integrity testing of spray-dried particles in a 10-kW chemical-looping combustor using natural gas as fuel. *Fuel*, 88(11):2083–2096, 2009.

[67] A. Cuadrat, A. Abad, J. Adánez, L. de Diego, F. García-Labiano, and P. Gayán. Behaviour of ilmenite as oxygen carrier in chemical-looping combustion. In *Clean Coal Technology Conference*, Dresden 2009.

[68] J. Adánez, A. Cuadrat, A. Abad, P. Gayán, L. de Diego, and F. García-Labiano. Ilmenite activation during consecutive redox cycles in chemical-looping combustion. *Energy Fuels*, 24(2):1402–1413, 2010.

[69] M. Rydén, M. Johansson, E. Cleverstam, A. Lyngfelt, and T. Mattisson. Ilmenite with addition of NiO as oxygen carrier for chemical-looping combustion. *Fuel*, 89 (11):3523–3533, 2010.

[70] P. Moldenhauer, M. Rydén, and A. Lyngfelt. Testing of minerals and industrial by-products as oxygen carriers for chemical-looping combustion in a circulating fluidized-bed 300W laboratory reactor. *Fuel*, 93:351–363, 2012.

[71] M. Rydén, C. Linderholm, P. Markström, and A. Lyngfelt. Release of gas phase O2 from ilmenite during chemical-looping combustion experiments. *Chemical Engineering & Technology*, 35(11):1968–1972, 2012.

[72] D. Kunii and O. Levenspiel. *Fluidization Engineering*. Butterworth-Heinemann, 2nd edition, 1991.

[73] W. N. Zhang, F. Johnsson, and B. Leckner. Fluid-dynamic boundary layers in CFB boilers. *Chemical Engineering Science*, 50(2):201–210, 1995.

[74] J. Villermaux. *Génie de la réaction chimique*. Lavoisier Tec & Doc, 2nd edition, 1995. pp. 190–193.

[75] P. Kolbitsch, T. Pröll, and H. Hofbauer. Modeling of a 120 kW chemical looping combustion reactor system using a Ni-based oxygen carrier. *Chemical Engineering Science*, 64:99–108, 2009.

[76] C. Y. Wen and S. Dutta. Rates of coal pyrolysis and gasification reactions. In C. Y. Wen and E. Stanley Lee, editors, *Coal Conversion Technology*, chapter 2, pages 80–81. Addison-Wesley Publishing Company, Inc., 1979.

[77] N. Berguerand, A. Lyngfelt, T. Mattisson, and P. Markström. Chemical-looping combustion of solid fuels in a 10 kWth unit. *Oil & Gas Science and Technology - Rev. IFP Energies nouvelles*, 66(2):181–191, 2011.

[78] H. Leion, A. Lyngfelt, M. Johansson, E. Jerndal, and T. Mattisson. The use of ilmenite as an oxygen carrier in chemical-looping combustion. *Chemical Engineering Research and Design*, 86:1017–1026, 2008.

[79] News announcement. FW to supply supercritical CFB boiler island. *Pump Industry Analyst*, 1:3, January 2006.

A

Startup and shutdown procedures for operation of the 100 kW system

A.1 Preparation

- Change the dirty Biltema-filters for the sample gas.
- If necessary, refill water to the two sample gas water seals.
- Clean the filter between the coal screw and the coal screw water seal.
- Fill water to the coal screw water seal (water pipe should be filled to 3/4).
- Change the heat exchanger filter and write date on the white label.
- Refill particles to CY2 (while fluidising LS2 and FR) to replace the lost part.
- Prepare the fuel tank with enough fuel.
- Blow high pressure air through the sample gas pipes to clear the path.
- Make sure the N_2 supply is enough for the experiment.
- Notify Akademiska Hus of the operation dates and use of compressed air.

A.2 Startup (day before operation)

- Calibrate the analysers.
- Close all the oven doors tight.
- Start the computer.
- Start the touch panel (switch on the back side).
- Set all knobs on the touch panel cabinet to automatic (ON).
- Set the steam generator main power to ON (ON = 1).
- Set the leftmost knob on the steam generator cabinet to ON.
- Open the valve for LS2.
- Open the two valves for the pressure tap sweep gas.
- Check to see that all the pressure tap rotameters are set to 0.4 L_n/min.
- Open the red valve for water through the heat exchanger (set to 10–15).

- Open the valve for water to the coal screw cooling.
- Open the valve for water cooling of the sample gas pipes.
- Open the valves for water to the spray coolers.
- Make sure that the main valve between the coal screws is closed.
- Close the two valves for the air cooling for faster warm-up.
- Start the host computer Labview application (shortcut on desktop).
- Start the touch panel Labview application (shortcut on desktop).
- Wait a minute to let all electronics connect.
- Write " Startup" in the comment field
- Press the "Save?"-button and wait a minute for a zero pressure baseline.
- Check in the save-folder that a new file has been created (do not open it).
- Set the flows LS1/LS2F/LS3/LS4/CS1/CS2/CS3/CS4/CR/FR/LS2/AR to 2/1/2/2/4/4/4/4/5/5/30/1660
- Set the two bottom heaters ("Trafo") to 1000℃.
- In Labview, set all ON/OFF switches to ON, except for K-tron feeder.
- Set the three oven heaters to 1000℃.
- Set air preheater 1&2 to 860℃.
- Set air preheater CA to 180℃.
- Make sure all override safety protocol buttons are set to OFF.
- Open the coal screw rotameter (close to the LS2 valve) to 30 L_n/min.
- Set the remaining two knobs on the steam generator cabinet to ON (require 30 min warm-up).
- Put up the safety enclosure line.
- Note the operation information on the whiteboard.
- Leave for the day.

A.3 Fuel start (day of operation)

- Make sure the T1–T6 temperatures all lie in the range 980–1000℃.
- Check to see if all pressure drops are ok.
- Take down the safety enclosure line.
- Open the two valves for the air cooling.
- Set the override safety protocol button for "oven" to ON.
- Press the "Save?"-button to set it to OFF.
- Write " Run" in the comment field.
- Press the "Save?"-button.
- Check in the save-folder that a new file has been created (do not open it).
- Set the steam temperature to 180℃ and wait till it stabilises.
- Open the coal screw rotameter (close to the LS2 valve) to 50 L_n/min.
- Check the water seal level on the floor above to see that it is stable.
- Open the valve at the N_2 gas tubes (LS2 now becomes fluidised with N_2).

- Open the small valve and rotameter on the fuel tank lid.
- Open the four main valves that provide air to the PCC.
- Step-by-step, switch from air to steam, beginning at LS1 and ending at FR.
- Check the FR flow and be prepared to compensate for condensation.
- Set the FR flow to 8 kg/h and wait for the system to stabilise.
- Set K-Tron feeder to 5 kg/h.
- Open the main valve between the coal screws (use protective gear).
- In Labview, set the K-Tron feeder switch to ON, starting the fuel feeding.
- Check again the water seal level on the floor above to see that it is ok.
- Check again the water levels in the two sample gas water seals.

A.4 Shutdown (day of operation)

- Set K-Tron feeder to 0 kg/h.
- Set the K-Tron feeder switch to OFF.
- Close the main valve between the coal screws (use protective gear).
- Close the small valve and rotameter on the fuel tank lid.
- Close the four main valves that provide air to the PCC.
- Close the valve at the N_2 gas tubes (LS2 now becomes fluidised with air).
- Wait a while for most of the char to burn out.
- Press the "Save?"-button to set it to OFF.
- Write " Shutdown" in the comment field.
- Press the "Save?"-button.
- Check in the save-folder that a new file has been created (do not open it).
- Step-by-step, switch from steam to air, beginning at LS1 and ending at FR.
- Await the final char burnout.
- Shutdown the two bottom heaters ("Trafo").
- Set the ovens, steam temperature, preheater 1, 2 and CA to 20°C.
- Set the oven, heating trace, preheater 1, 2 and CA switches to OFF.
- Set the two rightmost knobs on the steam generator cabinet to OFF.
- Set the AR flow to 600–1000 L_n/min.
- Set the flue gas fan to -0.1 kPa for faster cooling.
- Leave for the day.

A.5 Post-shutdown (day after operation)

- Make sure the T1–T6 temperatures all lie in the range 20–100℃.
- In Labview, set all of the remaining ON/OFF switches to OFF.
- Set the LS1-FR flow to -2 kg/h, while the LS2 and AR flow to 0 L_n/min.
- Press the “Save?”-button to set it to OFF.
- Press the “Stop”-button in the Labview application.
- Shut down Windows XP Embedded on the touch panel.
- Shut down the touch panel when notified (switch on the back side).
- Set all knobs on the touch panel cabinet, except for the main power and the evacuation fan, to OFF.
- Set the leftmost knob on the steam generator cabinet to OFF.
- Set the steam generator main power to OFF (OFF = 0).
- Close the valve for water to the coal screw cooling.
- Close the valve for water cooling of the sample gas pipes.
- Close the two valves for the pressure tap sweep gas.
- Close the coal screw rotameter (close to the LS2 valve).
- Close the valve for LS2.
- Close the red valve for water through the heat exchanger (set to 0).
- Recover the saved files to USB for analysis.
- Shut down the host computer.

Paper I

Paper II

Paper III

Paper IV

Paper V

Paper VI